The Chandra Survey of Extragalactic Sources in the 3cr Catalog: X-Ray Emission From Nuclei, Jets, and Hotspots in the Chandra Archival Observations

The Astrophysical Journal Supplement Series, 220:5 (14pp), 2015 September doi:10.1088/0067-0049/220/1/5

THE *CHANDRA* SURVEY OF EXTRAGALACTIC SOURCES IN THE 3CR CATALOG: X-RAY EMISSION FROM NUCLEI, JETS, AND HOTSPOTS IN THE *CHANDRA* ARCHIVAL OBSERVATIONS

F. Massaro[1,2], D. E. Harris[3], E. Liuzzo[4], M. Orienti[4], R. Paladino[4,5], A. Paggi[3], G. R. Tremblay[2], B. J. Wilkes[3], J. Kuraszkiewicz[3], S. A. Baum[6,7], and C. P. O'Dea[6,8]
[1] Dipartimento di Fisica, Università degli Studi di Torino, via Pietro Giuria 1, I-10125 Torino, Italy
[2] Yale Center for Astronomy and Astrophysics, Physics Department, Yale University, P.O. Box 208120, New Haven, CT 06520-8120, USA
[3] Smithsonian Astrophysical Observatory, 60 Garden Street, Cambridge, MA 02138, USA
[4] Istituto di Radioastronomia, INAF, via Gobetti 101, I-40129, Bologna, Italy
[5] Department of Physics and Astronomy, University of Bologna, V.le Berti Pichat 6/2, I-40127 Bologna, Italy
[6] University of Manitoba, Dept of Physics and Astronomy, Winnipeg, MB R3T 2N2, Canada
[7] Carlson Center for Imaging Science 76-3144, 84 Lomb Memorial Dr., Rochester, NY 14623, USA
[8] School of Physics and Astronomy, Rochester Institute of Technology, 84 Lomb Memorial Drive, Rochester, NY 14623, USA
Received 2015 March 29; accepted 2015 June 9; published 2015 September 1

ABSTRACT

As part of our program to build a complete radio and X-ray database of all Third Cambridge catalog extragalactic radio sources, we present an analysis of 93 sources for which *Chandra* archival data are available. Most of these sources have already been published. Here we provide a uniform re-analysis and present nuclear X-ray fluxes and X-ray emission associated with radio jet knots and hotspots using both publicly available radio images and new radio images that have been constructed from data available in the Very Large Array archive. For about 1/3 of the sources in the selected sample, a comparison between the *Chandra* and radio observations was not reported in the literature: we find X-ray detections of 2 new radio jet knots and 17 hotspots. We also report the X-ray detection of extended emission from the intergalactic medium for 15 galaxy clusters.

Key words: galaxies: active – radio continuum: galaxies – X-rays: general

Supporting material: figure set

1. INTRODUCTION

The first release of the Third Cambridge catalog (3C), performed at 159 MHz, was published in 1959 (Edge et al. 1959). In 1962, Bennett et al. revised the whole 3C catalog using observations at 178 MHz. This revised version (3CR) was considered to be a definitive list of the brightest radio sources in the northern hemisphere for many years. The flux limit of the 3CR catalog is set to 9 Jy at 178 MHz, and it covers the whole northern hemisphere above −5° in decl. Then, in 1985, Spinrad, Djorgovski, Marr, and Aguilar presented the last revised version of the Third Cambridge catalog (3CR; Bennett 1962), listing 298 extragalactic radio sources (see also Edge et al. 1959; Mackay 1971; Smith et al. 1976; Smith & Spinrad 1980), including new revised positions, redshifts, and magnitudes having 91% of the sources out of the Galactic plane (i.e., Galactic latitude $|b| > 10°$). Since then, several photometric and spectroscopic surveys have been carried out to obtain multifrequency coverage of the 3CR catalog. All of the 3CR sources at redshift $z < 0.3$ have already been observed with the *Hubble Space Telescope* (e.g., Chiaberge et al. 2000; Tremblay et al. 2009), and a near-infrared, optical, and ultraviolet survey for higher-redshift sources is still ongoing. A large fraction of the 3CR radio sources were also targets of the spectroscopic survey carried out with the Telescopio Nazionale Galileo (TNG; e.g., Buttiglione et al. 2009). Radio images with arcsecond resolution for the majority of the 3CR sources are available from the NRAO Very Large Array (VLA) Archive Survey (NVAS)[9] and from the MERLIN archive.[10] As a radio low-frequency catalog, the selection criteria for the 3CR are unbiased with respect to X-rays. Since it spans a wide range of redshift and radio power and has a vast multifrequency database of ground- and spaced-based observations for comparison, it is an ideal sample to investigate the properties of active galaxies.

Motivated by the large number of multifrequency observations already available for the 3CR sources, we have undertaken a project to ensure that each 3CR extragalactic source has at least an exploratory/snapshot *Chandra* observation. We have chosen to accomplish this goal in a step-wise strategy, working out in redshift with modest proposals each cycle to minimize the impact on the *Chandra* schedule. A description of our progress in this endeavor is given in the following sections.

In this paper, we present the X-ray analyses of most of the 3CR sources present in the *Chandra* archive that have not already been published with our standard procedures, i.e., the snapshot surveys (Massaro et al. 2010, 2012, 2013; F. Massaro et al. 2015, in preparation) and the 3CR sources in the XJET sample (Massaro et al. 2011). Our main goal is to provide a uniform analysis of all the archival observations. X-ray flux maps were constructed and compared with radio images to search for any X-ray emission associated with radio jet knots, hotspots, and lobes. In some cases, new radio images have been constructed from archival VLA data for comparison with the X-ray images. We report measurements of the X-ray nuclear emission for all of the sources in our sample, but we did not perform a detailed spectral analysis because most of them (i.e., >70%) have already been reported in the literature (see, e.g., Hardcastle et al. 2009; Balmaverde et al. 2012; Wilkes et al. 2013; J. Kuraszkiewicz et al. 2015, in preparation).

The paper is organized as follows. A brief historical overview of the *Chandra* observations of the 3CR sources is provided in Section 2, and a description of the selected sample

[9] http://archive.nrao.edu/nvas/
[10] http://www.jb.man.ac.uk/cgi-bin/merlin_retrieve.pl

Table 1
Summary of the 3CR Sources Analyzed in Our Previous Investigations

Program	Cycle	Proposal Number	Number of Sources	Redshift Range	References
3CR snapshot survey	9	09700745	30[a]	$z < 0.3$	Massaro et al. (2010)
XJET[b]	…	…	47	…	Massaro et al. (2011)
3CR snapshot survey	12	12700211	26	$z < 0.3$	Massaro et al. (2012)
3CR snapshot survey	13	13700190	19	$z < 0.5$	Massaro et al. (2013)
3CR snapshot survey	15	15700111	23	$z < 1.0$	F. Massaro et al. (2015, in preparation)
Archival project[b]	…	…	93	…	This work

Notes.
[a] The AO9 sample includes 3CR 346, which was re-observed in Cycle 12 because during Cycle 9 its *Chandra* observation was affected by high background (see Massaro et al. 2010, for details).
[b] The redshift ranges for both the archival and the XJET samples are unbounded with respect to selection.

is presented in Section 3. Data reduction procedures are given in Section 4, and the results are discussed in Section 5. Then, Section 6 is devoted to our summary and conclusions. Finally, we provide X-ray images with radio contours superposed for all of the sources analyzed (Appendix A) and a summary of the *Chandra* observations for the entire sample of 3CR extragalactic sources (Appendix B).

For numerical results, cgs units are used unless stated otherwise, and a flat cosmology was assumed with $H_0 = 72$ km s^{-1} Mpc^{-1}, $\Omega_M = 0.27$, and $\Omega_\Lambda = 0.73$ (Dunkley et al. 2009), to be consistent with our previous analyses (e.g., Massaro et al. 2010, 2012, 2013). Spectral indices, α, are defined by flux density, $S_\nu \propto \nu^{-\alpha}$.

2. HISTORY OF THE 3CR *CHANDRA* SURVEY

A large fraction of the X-ray studies of 3CR extragalactic sources observed with *Chandra* are biased toward observations of "favorite" X-ray bright sources or objects with well-known interesting features and/or peculiarities (e.g., sources in the center of bright galaxy clusters) rather than consisting of well-defined samples. However, to complete the X-ray coverage for the whole 3CR catalog and to obtain a complete and uniform multifrequency database of these extragalactic radio sources, during *Chandra* Cycle 9, we started an X-ray snapshot survey of 3CR sources previously unobserved by *Chandra*. Several subsets of the 3CR sample have been observed by other groups (e.g., Wilkes et al. 2013; J. Kuraszkiewicz et al. 2015, in preparation).

The 3CR extragalactic catalog includes 298 sources, 248 of which are already in the *Chandra* archive. Among those observed, we have already published 47 sources as part of the XJET project (Massaro et al. 2011)[11] and an additional 98 as part of our 3CR *Chandra* snapshot survey (Massaro et al. 2010, 2012, 2013). Here we publish an additional 93 sources from the *Chandra* archive. It is worth noting that of the remaining 50 sources unobserved by *Chandra*, half are unidentified, i.e., lacking an assigned optical counterpart, and thus are unclassified. Table 1 provides the references for the 145 sources we have already processed and published.

According to the redshift estimates reported in the 3CR catalog, the *Chandra* archive now contains all of the 3CR sources up to $z = 0.5$ (i.e., 150 sources), with only the following exceptions: 3CR 27 at $z = 0.184$, 3CR 69 at $z = 0.458$ (Hiltner & Roeser 2009), and 3CR 93 at $z = 0.357$, as confirmed by Ho & Minjin (2009).

[11] http://hea-www.cfa.harvard.edu/XJET/

3. SAMPLE SELECTION FOR 3CR ARCHIVAL OBSERVATIONS

In the present paper, we uniformly analyzed 93 3CR sources observed by *Chandra* that were not reported in our previous investigations. We excluded from the present archival analysis seven 3CR sources that have been extensively discussed in the literature and that have an accumulated exposure time greater than 80 ks each. The excluded sources are 3CR 66A (e.g., Abdo et al. 2011), 3CR 71 (alias NGC 1068; e.g., Brinkman et al. 2002), 3CR 84 (alias NGC 1275 or Perseus A; e.g., Fabian et al. 2003), 3CR 186 (Siemiginowska et al. 2010), 3CR 231 (alias M82; e.g., Griffiths et al. 2000), 3CR 317 (alias Abell 2052; e.g., Blanton et al. 2009), and 3CR 348 (alias Hercules A; e.g., Nulsen et al. 2005). In addition, we also did not select for our analysis the three cases 3CR 236, 3CR 326, and 3CR 386, since the PI of these observations is currently working on them (M. Birkinshaw 2015, private communication).

In Table 2 we list all 93 selected sources, their coordinates, redshift estimates, luminosity distance, the *Chandra* observation ID number, exposure times, and observing dates. In the same table, we also list the references where the *Chandra* observations were analyzed/presented.

4. DATA REDUCTION AND DATA ANALYSIS

The radio and X-ray data reduction and analysis procedures adopted in the present analysis were extensively described in Massaro et al. (2012, 2013) and references therein. Here we report only the basic details.

4.1. Radio Observations

Radio observations presented in this paper were retrieved from the publicly available websites of M. J. Hardcastle and C. C. Cheung, from the NVAS (National Radio Astronomy Observatory VLA Archive Survey), from NED (NASA Extragalactic Database), from the DRAGN website, or were constructed from data available in the VLA archives. A summary of the archival data used is reported in Table 3. To produce our final images, we calibrated the data with standard procedures using AIPS, edited the visibilities, and carried out a few self-calibration cycles. Image parameters for each figure are given in Appendix A.

Table 2
Source List of the Archival *Chandra* 3CR Radio Sources

3CR Name	R.A. (J2000) (hh mm ss)	decl. (J2000) (dd mm ss)	z	kpc Scale (kpc/arcsec)	D_L (Mpc)	*Chandra* Obs. and Proposal IDs	Obs. Date yyyy-mm-dd	Data Mode	Live Time ksec	References
2.0	00:06:22.6	−00:04:24.6	1.0374	7.999	6849.63	5617 (06700116)	2005 Jul 28	ACIS-S FAINT	16.93	Miller et al. (2011)
13.0	00:34:14.500	+39:24:17.00	1.351	8.357	9528.43	9241 (09700482)	2008 Jun 01	ACIS-S FAINT	19.53	Wilkes et al. (2013)
14.0	00:36:06.447	+18:37:59.08	1.469	8.412	10578.07	9242 (09700482)	2008 May 29	ACIS-S FAINT	3.00	Wilkes et al. (2013)
22.0	00:50:56.222	+51:12:03.26	0.936	7.792	6024.20	14994 (14700660)	2013 Jun 05	ACIS-S FAINT	9.35	J. Kuraszkiewicz et al. (2015, in preparation)
28.0	00:55:50.6	+26:24:36.7	0.1953	3.162	931.87	3233 (03800625)	2002 Oct 07	ACIS-I VFAINT	49.72	McCarthy et al. (2004), Donato et al. (2004)
35.0	01:12:02.288	+49:28:35.62	0.067	1.250	293.48	10240 (10700504)	2009 Mar 08	ACIS-I VFAINT	25.63	Isobe et al. (2011)
40.0	01:26:00.616	-01:20:42.44	0.018	0.356	75.99	7823 (08700576)	2007 Sep 07	ACIS-S VFAINT	64.82	Sun (2009)
43.0	01:29:59.776	+23:38:19.85	1.459	8.409	10488.44	9324 (09700482)	2008 Jun 17	ACIS-S FAINT	3.04	Wilkes et al. (2013)
48.0	01:37:41.301	+33:09:35.27	0.367	4.991	1923.58	3097 (03700781)	2002 Mar 06	ACIS-S VFAINT	9.22	Worrall et al. (2004)
49.0	01:41:09.159	+13:53:28.33	0.621	6.687	3837.59	14995 (14700660)	2013 Aug 31	ACIS-S FAINT	9.45	J. Kuraszkiewicz et al. (2015, in preparation)
65.0	02:23:43.1	+40:00:51.9	1.176	8.203	8011.89	9243 (09700482)	2008 Jun 30	ACIS-S FAINT	20.91	Wilkes et al. (2013)
68.1	02:32:28.8	+34:23:45.9	1.238	8.269	8543.36	9244 (09700482)	2008 Feb 10	ACIS-S FAINT	3.05	Wilkes et al. (2013)
68.2	02:34:23.8	+31:34:17.0	1.575	8.435	11537.52	9245 (09700482)	2008 Mar 06	ACIS-S FAINT	19.88	Wilkes et al. (2013)
75.0	02:57:41.570	+06:01:36.92	0.0232	0.456	98.33	4181 (04800347)	2003 Sep 19	ACIS-I VFAINT	21.49	Balmaverde et al. (2006), Hudson et al. (2006)
78.0	03:08:26.222	+04:06:39.26	0.0287	0.560	122.12	4157 (04700407)	2004 Jun 28	ACIS-S VFAINT	50.86	Harwood & Hardcastle (2012)
88.0	03:27:54.171	+02:33:42.24	0.0302	0.588	128.66	11977 (11800517)	2009 Oct 06	ACIS-S VFAINT	49.62	Sun (2009)
98.0	03:58:54.431	+10:26:02.72	0.0305	0.594	129.97	10234 (10700504)	2008 Dec 24	ACIS-I VFAINT	31.71	Hodges-Kluck et al. (2010)
99.0	04:01:07.6	+00:36:33.1	0.426	5.474	2296.01	5680 (06700612)	2005 Nov 28	ACIS-S FAINT	5.07	…
129.1	04:50:06.645	+45:03:05.91	0.0222	0.436	94.03	2219 (02800530)	2001 Jan 09	ACIS-I FAINT	9.63	Krawczynski (2002)
136.1	05:16:03.275	+24:58:25.68	0.064	1.198	279.75	9326 (09700606)	2008 Jan 11	ACIS-S FAINT	9.91	Balmaverde et al. (2012)
138.0	05:21:09.906	+16:38:22.16	0.759	7.273	4641.94	14996 (14700660)	2013 Mar 22	ACIS-S FAINT	2.00	J. Kuraszkiewicz et al. (2015, in preparation)
147.0	05:42:36.127	+49:51:07.19	0.545	6.276	3271.83	14997 (14700660)	2013 Aug 26	ACIS-S FAINT	2.00	J. Kuraszkiewicz et al. (2015, in preparation)
172.0	07:02:08.305	+25:13:53.52	0.519	6.119	3083.34	14998 (14700660)	2013 Sep 05	ACIS-S FAINT	9.95	J. Kuraszkiewicz et al. (2015, in preparation)
175.0	07:13:02.422	+11:46:16.25	0.77	7.312	4725.35	14999 (14700660)	2013 Feb 21	ACIS-S FAINT	2.00	J. Kuraszkiewicz et al. (2015, in preparation)
175.1	07:14:04.695	+14:36:22.57	0.92	7.754	5896.15	15000 (14700660)	2013 Feb 10	ACIS-S FAINT	9.94	J. Kuraszkiewicz et al. (2015, in preparation)
181.0	07:28:10.216	+14:37:36.60	1.382	8.375	9802.28	9246 (09700482)	2009 Feb 12	ACIS-S FAINT	3.02	Wilkes et al. (2013)
184.0	07:39:24.4	+70:23:10.0	0.994	7.917	6493.56	3226 (03800590)	2002 Sep 22	ACIS-S VFAINT	18.89	Belsole et al. (2004), Hardcastle et al. (2004)
190.0	08:01:33.552	+14:14:42.83	1.1956	8.225	8179.15	9247 (09700482)	2007 Dec 31	ACIS-S FAINT	3.06	Wilkes et al. (2013)
191.0	08:04:47.968	+10:15:23.72	1.956	8.375	15096.31	5626 (06700234)	2005 Dec 14	ACIS-S VFAINT	19.77	Erlund et al. (2006)
192.0	08:05:35.005	+24:09:50.36	0.0597	1.123	260.18	9270 (09700606)	2007 Dec 18	ACIS-S FAINT	10.02	Hodges-Kluck et al. (2010)
196.0	08:13:36.058	+48:13:02.66	0.871	7.627	5507.36	15001 (14700660)	2013 Mar 23	ACIS-S FAINT	2.00	J. Kuraszkiewicz et al. (2015, in preparation)
200.0	08:27:25.384	+29:18:45.01	0.458	5.711	2504.16	838 (01700549)	2000 Oct 06	ACIS-S FAINT	14.66	Hardcastle et al. (2004)
204.0	08:37:45.003	+65:13:35.34	1.112	8.119	7470.55	9248 (09700482)	2008 Jan 13	ACIS-S FAINT	3.05	Wilkes et al. (2013)
205.0	08:39:06.534	+57:54:17.09	1.534	8.429	11164.65	9249 (09700482)	2008 Jan 26	ACIS-S FAINT	9.67	Wilkes et al. (2013)
208.0	08:53:08.608	+13:52:54.85	1.1115	8.118	7466.35	9250 (09700482)	2008 Jan 08	ACIS-S FAINT	3.01	Wilkes et al. (2013)
210.0	08:58:10.0	+27:50:54.9	1.169	8.194	7952.27	5821 (06800802)	2004 Dec 25	ACIS-S VFAINT	20.57	Gilmour et al. (2009)
215.0	09:06:31.874	+16:46:11.81	0.4121	5.366	2206.92	3054 (03700563)	2003 Jan 02	ACIS-S FAINT	33.80	Hardcastle et al. (2004)
216.0	09:09:33.498	+42:53:46.51	0.6699	6.916	3978.18	15002 (14700660)	2013 Feb 25	ACIS-S FAINT	2.00	J. Kuraszkiewicz et al. (2015, in preparation)
220.1	09:32:40.025	+79:06:30.14	0.61	6.632	3545.74	839 (01700549)	1999 Dec 29	ACIS-S FAINT	18.92	Worrall et al. (2001)
220.3	09:39:23.4	+83:15:26.2	0.68	6.961	4052.36	14992 (14700660)	2013 Jan 21	ACIS-S FAINT	9.94	Haas et al. (2014)
226.0	09:44:16.522	+09:46:17.07	0.8177	7.471	5091.20	15003 (14700660)	2013 Oct 07	ACIS-S FAINT	9.94	J. Kuraszkiewicz et al. (2015, in preparation)
228.0	09:50:10.794	+14:20:00.68	0.5524	6.319	3141.17	2095 (02700363)	2001 Jun 03	ACIS-S FAINT	13.78	
241.0	10:21:54.6	+21:59:31.2	1.617	8.438	11921.71	9251 (09700482)	2008 Mar 13	ACIS-S FAINT	18.93	Wilkes et al. (2013)
245.0	10:42:44.609	+12:03:31.15	1.0279	7.982	6771.29	2136 (02700500)	2001 Feb 12	ACIS-S FAINT	10.40	Gambill et al. (2003)
249.1	11:04:13.842	+76:58:58.17	0.3115	4.474	1587.34	3986 (04700368)	2003 Jul 02	ACIS-I VFAINT	24.04	Stockton et al. (2006)
252.0	11:11:32.995	+35:40:41.50	1.1	8.102	7370.04	9252 (09700482)	2008 Mar 11	ACIS-S FAINT	19.45	Wilkes et al. (2013)
256.0	11:20:43.02	+23:27:55.2	1.819	8.417	13798.51	1660 (02800089)	2001 Apr 23	ACIS-I VFAINT	71.25	Vikhlinin et al. (2002)
263.1	11:43:25.094	+22:06:56.10	0.824	7.490	5140.19	15004 (14700660)	2013 Mar 20	ACIS-S FAINT	9.94	J. Kuraszkiewicz et al. (2015, in preparation)
266.0	11:45:43.30	+49:46:08.0	1.275	8.302	8863.60	9253 (09700482)	2008 Feb 16	ACIS-S FAINT	18.23	Wilkes et al. (2013)
267.0	11:49:56.506	+12:47:18.83	1.14	8.158	7706.55	9254 (09700482)	2008 Jul 07	ACIS-S FAINT	19.18	Wilkes et al. (2013)

Table 2
(Continued)

3CR Name	R.A. (J2000) (hh mm ss)	decl. (J2000) (dd mm ss)	z	kpc Scale (kpc/arcsec)	D_L (Mpc)	*Chandra* Obs. and Proposal IDs	Obs. Date yyyy-mm-dd	Data Mode	Live Time ksec	References
268.1	12:00:24.482	+73:00:45.81	0.97	7.868	6298.40	15005 (14700660)	2013 Jul 08	ACIS-S FAINT	9.94	J. Kuraszkiewicz et al. (2015, in preparation)
268.3	12:06:24.89	+64:13:37.9	0.3717	5.032	1952.68	10382 (10700678)	2009 Jul 29	ACIS-S VFAINT	42.53	…
268.4	12:09:13.610	+43:39:20.89	1.4022	8.385	9981.44	9325 (09700482)	2009 Feb 23	ACIS-S FAINT	3.02	Wilkes et al. (2013)
270.1	12:20:33.881	+33:43:11.99	1.5284	8.428	11113.88	9255 (09700482)	2008 Feb 16	ACIS-S FAINT	9.67	Wilkes et al. (2012)
277.1	12:52:26.353	+56:34:19.58	0.3198	4.556	1636.83	3102 (03700781)	2002 Oct 27	ACIS-S VFAINT	14.01	Siemiginowska et al. (2008)
277.3	12:54:12.010	+27:37:33.86	0.0853	1.559	378.60	11391 (11700216)	2010 Mar 03	ACIS-S VFAINT	24.80	Balmaverde et al. (2012)
285.0	13:21:17.868	+42:35:14.91	0.0794	1.461	351.00	6911 (07701073)	2006 Mar 18	ACIS-S VFAINT	39.62	Hardcastle et al. (2006)
286.0	13:31:08.292	+30:30:32.95	0.8499	7.760	5341.81	15006 (14700660)	2013 Feb 26	ACIS-S FAINT	2.00	J. Kuraszkiewicz et al. (2015, in preparation)
287.0	13:30:37.689	+25:09:10.96	1.055	7.567	6995.09	3103 (03700781)	2002 Jan 06	ACIS-S VFAINT	36.21	Siemiginowska et al. (2008)
288.0	13:38:49.9	+38:51:09.5	0.246	3.777	1209.42	9257(09700482)	2008 Apr 13	ACIS-S VFAINT	39.64	Hardcastle et al. (2007), Lal et al. (2010)
289.0	13:45:26.251	+49:46:32.47	0.9674	7.862	6643.17	15007 (14700660)	2013 Jul 28	ACIS-S FAINT	9.70	J. Kuraszkiewicz et al. (2015, in preparation)
298.0	14:19:08.18	+06:28:34.8	1.4381	8.401	10301.34	3104 (03700781)	2002 Mar 01	ACIS-S VFAINT	17.88	Siemiginowska et al. (2008)
299.0	14:21:05.631	+41:44:48.68	0.367	4.991	1923.58	12019 (10700678)	2009 Nov 08	ACIS-S VFAINT	39.53	…
309.1	14:59:07.58	+71:40:19.9	0.905	7.717	5776.46	3105 (03700781)	2002 Jan 28	ACIS-S VFAINT	16.95	
310.0	15:04:57.12	+26:00:58.5	0.0538	1.019	233.38	11845 (11700016)	2010 Apr 09	ACIS-S FAINT	57.58	Kraft et al. (2012)
318.0	15:20:05.484	+20:16:05.75	1.574	8.435	11528.39	9256 (09700482)	2008 May 05	ACIS-S FAINT	9.78	Wilkes et al. (2013)
318.1	15:21:51.9	+07:42:31.9	0.0453	0.867	195.26	900 (01800303)	2000 Apr 03	ACIS-I VFAINT	57.32	Mazzotta et al. (2002)
324.0	15:49:48.811	+21:25:38.34	1.2063	8.237	8270.74	326 (01600145)	2000 Jun 25	ACIS-S VFAINT	42.18	Boschin (2002)
325.0	15:49:58.421	+62:41:21.57	1.135	8.151	7664.22	6267 (05700521)	2005 Apr 14	ACIS-S VFAINT	29.65	Salvati et al. (2008)
334.0	16:20:21.819	+17:36:23.90	0.5551	6.335	3159.91	2097 (02700363)	2001 Aug 22	ACIS-S FAINT	32.47	Hardcastle et al. (2004)
336.0	16:24:39.090	+23:45:12.23	0.9265	7.769	5948.01	15008 (14700660)	2013 Mar 03	ACIS-S FAINT	2.00	J. Kuraszkiewicz et al. (2015, in preparation)
337.0	16:28:52.569	+44:19:06.58	0.635	6.755	3724.80	15009 (14700660)	2013 Oct 05	ACIS-S FAINT	9.95	J. Kuraszkiewicz et al. (2015, in preparation)
338.0	16:28:38.240	+39:33:04.14	0.0304	0.592	129.53	10748 (10800906)	2009 Nov 19	ACIS-I VFAINT	40.58	Kirkpatrick et al. (2011), Nulsen et al. (2013)
340.0	16:29:36.591	+23:20:12.83	0.7754	7.331	4766.4	15010 (14700660)	2013 Oct 20	ACIS-S FAINT	9.95	J. Kuraszkiewicz et al. (2015, in preparation)
343.0	16:34:33.809	+62:45:35.89	0.988	7.905	6444.64	15011 (14700660)	2013 Apr 28	ACIS-S FAINT	9.94	J. Kuraszkiewicz et al. (2015, in preparation)
343.1	16:38:28.203	+62:34:44.29	0.75	7.240	4573.74	15012 (14700660)	2013 Feb 25	ACIS-S FAINT	9.94	J. Kuraszkiewicz et al. (2015, in preparation)
352.0	17:10:44.138	+46:01:28.47	0.8067	7.436	5006.3	15013 (14700660)	2013 Oct 10	ACIS-S FAINT	9.95	J. Kuraszkiewicz et al. (2015, in preparation)
356.0	17:24:19.041	+50:57:40.14	1.079	8.069	7194.59	9257 (09700482)	2008 Jan 20	ACIS-S FAINT	19.87	Wilkes et al. (2013)
368.0	18:05:06.3	+11:01:32.0	1.131	8.146	7630.44	9258 (09700482)	2008 Jun 01	ACIS-S FAINT	19.91	Wilkes et al. (2013)
382.0	18:35:03.387	+32:41:46.85	0.0579	1.092	251.98	6151 (05701042)	2004 Oct 30	ACIS-S FAINT	63.87	Gliozzi et al. (2007)
388.0	18:44:02.374	+45:33:29.56	0.0917	1.663	408.83	5295 (05700009)	2004 Jan 29	ACIS-I VFAINT	30.71	Kraft et al. (2006)
401.0	19:40:25.039	+60:41:36.05	0.2011	3.236	962.99	4370 (03700685)	2002 Sep 21	ACIS-S FAINT	24.85	Reynolds et al. (2005)
427.1	21:04:06.966	+76:33:10.28	0.572	6.430	3277.55	2194 (02700664)	2002 Jan 27	ACIS-S FAINT	39.45	Hardcastle et al. (2004), Belsole et al. (2007)
432.0	21:22:46.327	+17:04:37.96	1.785	8.424	13479.35	5624 (06700234)	2005 Jan 07	ACIS-S VFAINT	19.78	Erlund et al. (2006)
433.0	21:23:44.582	+25:04:27.63	0.1016	1.823	456.17	7881 (08700989)	2007 Aug 28	ACIS-S VFAINT	37.17	Miller & Brandt (2009)
437.0	21:47:25.265	+15:20:32.03	1.48	8.415	10677.05	9259 (09700482)	2008 Jan 07	ACIS-S FAINT	19.88	Wilkes et al. (2013)
438.0	21:55:52.269	+38:00:28.33	0.29	4.257	1460.96	12879 (12800244)	2011 Jan 28	ACIS-S VFAINT	72.04	Hardcastle et al. (2004)
441.0	22:06:04.90	+29:29:20.0	0.708	7.078	4259.10	15656 (14700660)	2013 Jun 26	ACIS-S FAINT	6.98	J. Kuraszkiewicz et al. (2015, in preparation)
442.0	22:14:46.894	+13:50:27.13	0.0263	0.515	111.71	6392 (06700371)	2005 Oct 07	ACIS-I VFAINT	32.69	Worrall et al. (2007), Hardcastle et al. (2007)
449.0	22:31:20.582	+39:21:29.53	0.0171	0.338	72.12	13123 (11800387)	2010 Sep 20	ACIS-S VFAINT	59.92	Lal et al. (2013)
455.0	22:55:03.91	+13:13:35.0	0.543	6.264	3249.99	15014 (14700660)	2013 Aug 13	ACIS-S FAINT	9.95	J. Kuraszkiewicz et al. (2015, in preparation)
469.1	23:55:23.034	+79:55:18.28	1.336	8.348	9396.53	9260 (09700482)	2009 May 24	ACIS-S FAINT	19.91	Wilkes et al. (2013)
470.0	23:58:35.910	+44:04:45.51	1.653	8.439	12252.68	9261 (09700482)	2008 Mar 03	ACIS-S FAINT	19.91	Wilkes et al. (2013)

Notes. Col. (1): the 3CR name. Col. (2): R.A. and decl. (equinox J2000) of the radio position used to perform the registration (see Section 4 for details). We reported here the original 3CR position (Spinrad et al. 1985) of the sources for which the radio core was not clearly detected. Col. (3): redshift z. We also verified in the literature (e.g., NED and/or SIMBAD databases) if new z values were reported after the release of the 3CR catalog. Col. (4): the angular to linear scale factor in arcseconds. Cosmological parameters used to compute it are reported in Section 1. Col. (5): luminosity distance in Mpc. Cosmological parameters used to compute it are reported in Section 1. Col. (6): *Chandra* observation identification number. Proposal identification number is also reported in parentheses. Col. (7): *Chandra* observation date. Col. (8): data mode indicates how the *Chandra* ACIS detector was configured for the observation analyzed. Col. (9): the live time of the *Chandra* observation. Col. (10): the reference for the *Chandra* observation.

Table 3
Summary of Radio Observations

Name	NRAO Project ID	Freq (GHz)	Time on Source (s)	HPBW (arcsec × arcsec)
3CR 210	AO230	1.42	1200	1.66 × 1.62
3CR 256	AM224	4.76	180	1.72 × 1.35
3CR 267	AL330	8.44	1620	0.81 × 0.74
3CR 277.1	AV231	22.46	360	0.097 × 0.080
3CR 437	AV164	4.86	1500	1.22 × 1.17
3CR 470	AL330	8.46	1780	1.54 × 1.27

Notes. Col. (1): the 3CR name. Col. (2): the identification number of the observer program, as reported in the header of the raw u,v data downloaded from the VLA archive (see https://archive.nrao.edu/archive/nraodashelpj.html for more details). Col. (3): the frequency at which the radio observations were performed. Col. (4): the total exposure in seconds. Col. (5): the half-power beam width (HPBW) of the reduced radio images.

4.2. X-Ray Observations

The data reduction was performed following the standard procedure described in the *Chandra* Interactive Analysis of Observations (CIAO) threads,[12] using CIAO v4.6 and the *Chandra* Calibration Database (CALDB) version 4.6.2. Level 2 event files were generated using the *acis_process_events* task, and events were filtered for grades 0, 2, 3, 4, and 6. Light curves were also extracted for every data set, thus confirming the absence of high background intervals. Astrometric registration was achieved by aligning the nuclear X-ray position with that of the radio (see, e.g., Massaro et al. 2010, 2011).

Three different flux maps were created in the energy ranges 0.5–1 keV (soft), 1–2 keV (medium), and 2–7 keV (hard). Flux maps, as implemented in CIAO, are corrected for exposure time and effective area, and our implementation used monochromatic exposure maps. Each band is assigned a nominal energy; in our case, the nominal energies are 0.75, 1.4, and 4 keV for the soft, medium, and hard bands, respectively, and the exposure maps are constructed for these nominal values. Since the natural units of X-ray flux maps are counts s^{-1} cm^{-2}, we converted them to cgs units by multiplying each event by the nominal energy of its band, thereby assuming that every event in the band has the same energy. However, when we perform our photometry, we make the necessary correction to recover the observed erg cm^{-2} s^{-1}. The use of the "nominal energy" is only to obtain the correct units. The total energy for any particular region is recovered by applying a correction factor of E (average)/E (nominal) to the photometric measurement. To derive E(average), the actual values were measured with the CIAO tool *dmstat*. This correction ranged from a few percent to 15%.

To measure the observed fluxes for the nuclear emission, as well as for any feature, a region of size and shape appropriate to the observed X-ray emission was chosen. Two background regions, each with the same shape and size, were chosen so as to avoid emission from other parts of the source and to sample both sides of jet features or two areas close to hotspots. The flux in any particular band for any particular region was measured using funtools[13] (see also Massaro et al. 2011).

A 1σ error is calculated based on the usual $\sqrt{\text{number-of-counts}}$ in the source and background regions. The fluxes reported here are not corrected for Galactic absorption. X-ray fluxes measured for the cores are reported in Table 4, while those for the radio jet knots and hotspots detected are given in Table 5.

At the focal point, the *Chandra* mirrors produce an image of a point source with an FWHM of the order of $0''.7$. Since the native ACIS pixel size is $0''.492$, the data are undersampled. To recover the resolution inherent in the telescope, we normally regrid our images with binning factors of 1/2, 1/4, or 1/8 of the native ACIS pixel size. The choice of binning factor was dictated by the angular size of the radio source and by the number of counts in source components. The fact that the telescope dithers during each observation, together with the fact that real numbers rather than integers are used throughout for event location, permits us to achieve adequate Nyquist sampling of the point-spread function (PSF). For sources of large angular extent, 1/2 or no regridding was used (see also Massaro et al. 2012, 2013, for more details).

5. RESULTS

X-ray emission was clearly detected for 85 out of 93 nuclei in our sample. For 3CR 441, we did not perform X-ray photometry since the number of counts measured within a circular region of $2''$ centered on the radio position is consistent with the background. For an additional four sources, namely, 3CR 99, 3CR 220.3, 3CR 256, and 3CR 368, we measured too few X-ray counts to define a discrete nucleus in the *Chandra* image. In the three sources 3CR 28, 3CR 288, and 3CR 310, we could not measure the X-ray flux because the extended emission from the cluster washes out the discrete nuclear emission. For all of the other sources, the nuclear X-ray fluxes in the three bands (see Section 4.2), together with their X-ray luminosities, are reported in Table 4.

A detailed spectral analysis for the bright cores is beyond the scope of this paper since a large fraction of the sources were extensively analyzed in the literature. As in our previous investigations, in Table 4, we also report an "extended emission" parameter computed as the ratio of the net counts in the $r = 2''$ circle to the net counts in the $r = 10''$ circular region surrounding the core of each 3CR source (i.e., Ext. Ratio "Extent Ratio"). Values significantly less than 0.9 indicate the presence of extended emission around the nuclear component (e.g., Massaro et al. 2010, 2013).

We detected and report here the X-ray emission of 8 radio jet knots in 7 sources and 17 hotspots in 13 objects; no emission arising from lobes was found. To the best of our knowledge, two of our jet knot detections (3CR 78 and 3CR 245) and all of the hotspots had not previously been reported in the literature.

X-ray fluxes for radio jet knots and hotspots found in the 3CR sample are reported in Table 5, where the classification of each component is also provided. The significance of all detections is above 5σ, with the exception of the northern hotspot in 3CR 470 (i.e., n14.4), which corresponds to a $\sim 1\sigma$ detection. These significances have been computed assuming a Poisson distribution for the background as in Massaro et al. (2013).

In our sample, there are also 15 sources, members of galaxy clusters, for which extended X-ray emission is clearly visible, all previously known as cluster-related X-ray sources. For each galaxy cluster in our sample, we present the basic parameters in

[12] http://cxc.harvard.edu/ciao/guides/index.html
[13] http://www.cfa.harvard.edu/~john/funtools

Table 4
X-Ray Emission from Radio Cores

3CR Name	Net Counts	Ext. Ratio	$F_{0.5-1\,\mathrm{keV}}$[a] (cgs)	$F_{1-2\,\mathrm{keV}}$[a] (cgs)	$F_{2-7\,\mathrm{keV}}$[a] (cgs)	$F_{0.5-7\,\mathrm{keV}}$[a] (cgs)	L_X (10^{44} erg s^{-1})
2.0	839 (29)	0.34 (0.02)	77.79 (7.04)	125.34 (6.16)	291.05 (17.06)	494.18 (19.45)	31.07 (1.22)
13.0	14 (4)	0.50 (0.18)	0.79 (0.4)	0.88 (0.4)	3.02 (1.51)	4.69 (1.61)	0.57 (0.2)
14.0	228 (15)	0.94 (0.09)	59.38 (8.38)	129.09 (12.48)	314.41 (37.58)	502.88 (40.47)	75.48 (6.07)
22.0	64 (8)	0.83 (0.14)	0.0 (0.0)	4.82 (1.64)	95.56 (13.0)	100.38 (13.11)	4.9 (0.64)
35.0	12 (3)	0.61 (0.24)	0.0 (0.0)	1.14 (0.47)	2.93 (1.19)	4.07 (1.28)	0.0005 (0.0002)
40.0	2443 (49)	0.54 (0.02)	80.69 (2.21)	35.59 (1.45)	95.95 (4.95)	212.24 (5.61)	0.00146 (0.00004)
43.0	162 (13)	0.98 (0.11)	42.9 (6.78)	87.82 (10.28)	216.29 (30.59)	347.0 (32.97)	52.17 (4.96)
48.0[b]	5814 (76)	0.96 (0.02)	699.0 (14.02)	808.37 (17.05)	1514.14 (46.08)	3021.51 (51.09)	15.0 (0.25)
49.0	156 (12)	0.96 (0.11)	0.31 (0.7)	23.32 (3.33)	162.79 (15.66)	186.42 (16.03)	3.28 (0.28)
65.0	196 (14)	0.05 (0.02)	0.89 (0.4)	13.46 (1.6)	77.54 (7.09)	91.9 (7.28)	7.91 (0.63)
68.1	41 (6)	0.9 (0.19)	4.85 (2.42)	18.1 (4.84)	115.99 (24.18)	138.93 (24.78)	13.6 (2.43)
68.2	9 (3)	0.28 (0.12)	0.21 (0.21)	0.37 (0.26)	5.08 (2.07)	5.66 (2.1)	1.01 (0.37)
75.0	219 (15)	0.79 (0.07)	23.62 (2.87)	14.86 (1.73)	57.96 (6.81)	96.44 (7.59)	0.0013 (0.0001)
78.0[b]	20856 (144)	0.92 (0.01)	432.13 (5.1)	647.73 (6.62)	1004.17 (15.55)	2084.03 (17.65)	0.0396 (0.0003)
88.0	659 (26)	0.6	3.23 (0.61) (0.03)	18.44 (1.24)	109.08 (5.59)	130.75 (5.76)	0.0029 (0.0001)
98.0	1245 (35)	0.93 (0.04)	6.06 (1.24)	9.53 (1.19)	682.98 (20.18)	698.57 (20.26)	0.0153 (0.0004)
129.1	14 (4)	0.22 (0.06)	0.87 (0.87)	4.45 (1.51)	0.7 (2.27)	6.03 (2.86)	7.02e-5 (3.33e-5)
136.1	6 (2)	0.17 (0.17)	0.53 (0.53)	0.54 (0.38)	5.57 (3.22)	6.64 (3.28)	0.0007 (0.0003)
138.0[b]	385 (20)	0.96 (0.07)	116.59 (16.7)	330.91 (25.32)	1232.66 (96.62)	1680.17 (101.27)	48.56 (2.93)
147.0	150 (12)	0.99 (0.11)	44.12 (10.7)	160.22 (17.8)	341.21 (47.89)	545.54 (52.2)	6.99 (0.67)
172.0	26 (5)	0.70 (0.18)	0.0 (0.0)	1.81 (0.91)	43.38 (9.09)	45.19 (9.13)	0.51 (0.1)
175.0[b]	355 (19)	0.95 (0.07)	160.43 (19.35)	308.97 (24.35)	831.95 (75.32)	1301.35 (81.49)	38.73 (2.43)
175.1	86 (9)	0.89 (0.13)	4.91 (1.55)	16.32 (2.56)	43.87 (7.66)	65.1 (8.23)	3.04 (0.38)
181.0	166 (13)	0.96 (0.10)	55.43 (7.86)	91.52 (10.51)	181.96 (29.52)	328.91 (32.3)	42.39 (4.16)
184.0	38 (6)	0.75 (0.16)	0.72 (0.32)	0.86 (0.38)	21.92 (4.07)	23.5 (4.1)	1.33 (0.23)
190.0	165 (13)	0.96 (0.10)	49.91 (7.72)	96.73 (10.62)	150.5 (24.1)	297.14 (27.44)	26.74 (2.47)
191.0	715 (27)	0.95 (0.05)	32.66 (2.25)	57.13 (3.17)	121.57 (9.04)	211.37 (9.84)	64.62 (3.01)
192.0	46 (7)	0.72 (0.15)	1.77 (0.72)	3.15 (1.13)	52.72 (9.83)	57.64 (9.92)	0.0511 (0.0009)
196.0	87 (9)	0.90 (0.13)	10.4 (5.2)	87.35 (13.75)	297.91 (45.97)	395.67 (48.26)	16.1 (1.96)
200.0	202 (14)	0.81 (0.08)	11.55 (1.36)	19.61 (2.1)	32.8 (5.19)	63.97 (5.76)	0.54 (0.05)
204.0[b]	343 (19)	0.96 (0.07)	114.07 (11.21)	190.04 (14.9)	301.77 (35.56)	605.89 (40.15)	45.36 (3.01)
205.0[b]	969 (31	0.95 (0.04)	83.36 (5.42)	160.57 (7.62)	381.82 (22.71)	625.75 (24.56)	104.63 (4.11)
208.0	260 (16)	0.98 (0.09)	81.55 (9.68)	135.04 (12.54)	314.41 (36.8)	531.0 (40.06)	39.57 (2.99)
210.0	28 (5)	0.31 (0.08)	0.07 (0.16)	1.7 (0.54)	15.04 (3.67)	16.82 (3.72)	1.43 (0.32)
215.0[b]	11445 (107)	0.96 (0.01)	306.26 (5.02)	480.6 (6.97)	1140.72 (21.07)	1927.58 (22.75)	12.51 (0.15)
216.0[b]	244 (16)	0.97 (0.09)	134.19 (17.93)	203.98 (19.72)	553.56 (62.16)	891.73 (67.63)	18.94 (1.44)
220.1	1072 (33)	0.79 (0.03)	49.97 (2.44)	70.94 (3.55)	162.57 (10.71)	283.48 (11.55)	4.98 (0.2)
226.0	54 (7)	0.83 (0.15)	0.63 (0.63)	4.33 (1.46)	64.42 (9.97)	69.38 (10.09)	2.41 (0.35)
228.0	338 (18)	0.93 (0.07)	19.88 (1.9)	34.71 (2.88)	79.68 (8.92)	134.28 (9.57)	1.77 (0.13)
241.0	146 (12)	1.00 (0.12)	1.75 (0.58)	13.25 (1.61)	48.95 (5.89)	63.96(6.14)	12.19 (1.17)
245.0	1835 (43)	0.94 (0.03)	154.08 (6.21)	264.18 (9.48)	608.4 (29.24)	1026.67 (31.37)	63.31 (1.93)
249.1[b]	4367 (66)	0.96 (0.02)	252.12 (8.42)	322.33 (7.58)	1041.37 (25.72)	1615.82 (28.11)	5.44 (0.09)
252.0	86 (9)	0.64 (0.09)	0.19 (0.19)	4.25 (0.94)	51.24 (6.52)	55.67 (6.59)	4.08 (0.48)
263.1	430 (21)	0.96 (0.07)	52.7 (5.0)	70.61 (5.15)	180.43 (15.76)	303.74 (17.32)	10.77 (0.61)
266.0	19 (4)	1.07 (0.42)	0.5 (0.29)	0.81 (0.41)	9.29 (2.68)	10.61 (2.73)	1.12 (0.29)
267.0	166 (13)	0.89 (0.10)	0.88 (0.4)	10.0 (1.41)	81.65 (7.83)	92.53 (7.97)	7.37 (0.63)
268.1	46 (7)	0.94 (0.20)	0.4 (0.4)	1.21 (0.88)	60.37 (9.31)	61.98 (9.36)	3.32 (0.5)
268.3	398 (20)	0.98 (0.07)	1.3 (0.3)	4.57 (0.66)	117.52 (6.54)	123.4 (6.58)	0.63 (0.03)
268.4	282 (17)	0.98 (0.08)	78.15 (9.55)	145.82 (12.99)	375.22 (40.28)	599.19 (43.39)	79.76 (5.78)
270.1[b]	691 (26)	0.94 (0.05)	69.18 (4.89)	120.54 (6.72)	219.62 (17.11)	409.34 (19.02)	66.79 (3.1)
277.1	2287 (48)	0.95 (0.03)	167.79 (5.7)	225.01 (7.37)	468.66 (21.27)	861.45 (23.22)	3.1 (0.08)
277.3	229 (15)	0.81 (0.07)	1.38 (0.5)	4.28 (0.83)	140.84 (10.18)	146.5 (10.22)	0.028 (0.002)
285.0	457 (21)	0.87 (0.06)	0.34 (0.2)	1.44 (0.38)	216.95 (10.38)	218.73 (10.39)	0.036 (0.002)
286.0	117 (11)	0.96 (0.12)	87.64 (14.08)	100.04 (13.74)	158.45 (31.69)	346.14 (37.3)	13.21 (1.42)
287.0	3424 (59)	0.97 (0.02)	95.29 (2.62)	129.05 (3.45)	245.11 (9.29)	469.45 (10.25)	30.81 (0.67)
289.0	52 (7)	0.75 (0.13)	0.0 (0.0)	3.01 (1.37)	78.49 (11.63)	81.5 (11.71)	4.3 (0.62)
298.0[b]	9993 (100)	0.97 (0.01)	493.95 (8.59)	821.4 (12.42)	1660.05 (34.61)	2975.41 (37.76)	424.2 (5.38)
299.0	81 (9)	0.77 (0.12)	0.9 (0.28)	0.53 (0.22)	30.86 (3.81)	32.29 (3.82)	0.16(0.02)
309.1[b]	5254 (72)	0.97 (0.02)	259.9 (6.33)	423.95 (9.19)	1145.75 (30.3)	1829.6 (32.29)	81.67 (1.44)
318.0	256 (16)	0.96 (0.08)	23.6 (2.87)	43.99 (4.0)	89.4 (11.0)	156.99 (12.05)	4.43 (0.34)
318.1	106 (10)	0.071 (0.004)	2.79 (0.99)	4.82 (1.09)	3.97 (2.37)	11.57 (2.79)	0.0006 (0.0002)

Table 4
(Continued)

3CR Name	Net Counts	Ext. Ratio	$F_{0.5-1\,\mathrm{keV}}$ [a] (cgs)	$F_{1-2\,\mathrm{keV}}$ [a] (cgs)	$F_{2-7\,\mathrm{keV}}$ [a] (cgs)	$F_{0.5-7\,\mathrm{keV}}$ [a] (cgs)	L_X (10^{44} erg s^{-1})
324.0	40 (6)	0.61 (0.14)	0.64 (0.18)	0.92 (0.27)	5.48 (1.49)	7.05 (1.52)	0.65 (0.14)
325.0	365 (19)	0.86 (0.06)	2.6 (0.57)	19.23 (1.58)	93.96 (6.8)	115.79 (7.01)	4.56 (0.28)
334.0[b]	7178 (85)	0.96 (0.02)	203.45 (3.98)	292.96 (5.48)	684.21 (16.74)	1180.62 (18.06)	15.81 (0.24)
336.0[b]	191 (14)	0.95 (0.10)	98.63 (15.04)	184.79 (19.01)	343.29 (47.61)	626.71 (53.42)	29.78 (2.54)
337.0	9 (3)	0.53 (0.23)	0.0 (0.0)	1.1 (0.79)	11.33 (4.28)	12.43 (4.35)	0.23 (0.08)
338.0	246 (16)	0.092 (0.005)	16.48 (2.67)	13.33 (2.08)	12.17 (3.91)	41.97 (5.17)	0.0009 (0.0001)
340.0	86 (9)	0.92 (0.14)	1.46 (0.86)	11.56 (2.32)	84.78 (11.25)	97.8 (11.52)	2.98 (0.35)
343.0	18 (4)	0.76 (0.25)	2.88 (1.18)	2.46 (1.02)	6.61 (2.96)	11.95 (3.34)	0.67 (0.19)
343.1	47 (7)	1.04 (0.22)	3.02 (1.23)	9.88 (2.06)	25.2 (6.15)	38.09 (6.6)	1.07 (0.19)
352.0	129 (11)	0.88 (0.11)	2.57 (1.31)	22.66 (3.21)	95.99 (11.47)	121.22 (11.98)	4.05 (0.4)
356.0	24 (5)	0.38 (0.09)	0.35 (0.33)	0.73 (0.43)	13.24 (3.12)	14.32 (3.17)	0.99 (0.22)
382.0[b]	14052 (119)	0.86 (0.01)	72.82 (1.91)	174.65 (3.14)	2363.24 (24.23)	2610.71 (24.5)	0.215 (0.002)
388.0	271 (16)	0.28 (0.02)	20.53 (2.4)	19.15 (1.82)	19.28 (3.63)	58.96 (4.71)	0.013 (0.001)
401.0	229 (15)	0.34 (0.02)	9.48 (1.12)	12.35 (1.44)	26.96 (3.96)	48.79 (4.36)	0.06 (0.01)
427.1	18 (4)	0.22 (0.05)	0.24 (0.16)	0.24 (0.24)	4.85 (1.56)	5.33 (1.59)	0.08 (0.02)
432.0	730 (27)	0.93 (0.05)	34.32 (2.33)	57.96 (3.23)	120.42 (8.81)	212.7 (9.67)	53.29 (2.42)
433.0[b]	2724 (52)	0.92 (0.02)	2.69 (0.55)	13.24 (1.25)	1139.84 (22.48)	1155.78 (22.52)	0.32 (0.01)
437.0	7 (3)	0.43 (0.19)	0.2 (0.2)	0.37 (0.26)	4.1 (2.09)	4.67 (2.12)	0.71 (0.32)
438.0	162 (13)	0.1 (0.01)	1.2 (0.38)	3.62 (0.62)	14.83 (2.22)	19.65 (2.34)	0.06 (0.01)
442.0	181 (13)	0.58 (0.06)	3.08 (0.99)	13.86 (1.53)	41.91 (4.58)	58.85 (4.93)	0.00096 (8e-5)
449.0	558 (24)	0.54 (0.03)	12.81 (0.97)	13.41 (0.95)	31.81 (2.77)	58.02 (3.08)	0.0004 (2e-5)
455.0	150 (12)	0.96 (0.11)	13.61 (2.62)	29.18 (3.39)	64.09 (9.16)	106.88 (10.11)	1.35 (0.13)
469.1	77 (9)	0.72 (0.11)	0.32 (0.23)	2.66 (0.78)	47.29 (6.02)	50.27 (6.07)	5.95 (0.72)
470.0	54 (7)	0.76 (0.14)	0.0 (0.0)	1.46 (0.61)	35.08 (5.06)	36.54 (5.1)	7.36 (1.03)

Notes. Col. (1): the 3CR name. Col. (2): the net counts. The 1σ uncertainties, reported in parentheses, are computed assuming a Poisson distribution. Col. (3): the Ext. Ratio defined as the ratio of the net counts in the $r = 2''$ circle to the net counts in the $r = 10''$ circular region surrounding the core of each 3CR source. The 1σ uncertainties, reported in parentheses, are computed assuming a Poisson distribution. Col. (4): measured X-ray flux between 0.5 and 1 keV. Col. (5): measured X-ray flux between 1 and 2 keV. Col. (6): measured X-ray flux between 2 and 7 keV. Col. (7): measured X-ray flux between 0.5 and 7 keV. Col. (8): X-ray luminosity in the range 0.5–7 keV, with the 1σ uncertainties given in parentheses.
[a] Fluxes are given in units of 10^{-15} erg cm^{-2} s^{-1}, and 1σ uncertainties are given in parentheses. The uncertainties on the flux measurements were computed as described in Section 4.2.
[b] Sources having count rates above the threshold of 0.1 counts per frame for which the X-ray flux measurements is affected by pileup (see Massaro et al. 2013, and references therein for additional details).

Table 6: the associated 3CR radio source, the alternative X-ray or optical name if it was a known galaxy cluster, the size of the X-ray emission estimated as the radius of a circular region surrounding its emission, both in arcseconds and in kiloparsecs, together with the number of counts within the same area. A dedicated analysis of the 3CR sources in galaxy clusters, listed in the *Chandra* snapshot survey, will be presented in a future paper.

All of the X-ray images for the selected sample are presented in Appendix A.

6. SUMMARY AND CONCLUSIONS

We have described the combined radio–X-ray analyses of 93 3CR radio sources for which *Chandra* observations, requested by others for many different reasons, were already present in the archive. The main objectives of the present analysis are (1) to present a uniform X-ray and radio database for the 3CR catalog; (2) to search for possible detections of X-ray emission from radio jet knots, hotspots, and lobes; and (3) to look for new galaxy cluster detections surrounding the 3CR radio sources.

In order to perform the radio–X-ray comparison, we reduced archival radio observations for six sources. We focused on the comparison between the radio and X-ray emission from extended components such as radio jet knots, hotspots, and lobes. We discovered 2 new radio jet knots and 17 hotspots emitting in the X-ray. Flux maps for all of the X-ray observations were constructed, and we provided photometric results for all of the extended components detected.

All of the radio knots and hotspots have been classified on the basis of the radio morphology of their parent source, adopting the definition suggested by Leahy et al. (1997) for the hotspots, i.e., brightness peaks that are neither the core nor a part of the jet, usually lying where the jet terminates, and considering all other discrete brightness enhancements as jet knots.

The following conventions for labeling the extended structures detected in the X-rays were adopted. We indicated with the letter "k" the jet knots and with "h" the hotspots; then, the name of each component is a combination of one letter (indicating the cardinal direction of the radio feature with respect to the nucleus) and one number (indicating the distance from the core in arcsec) as described in Massaro et al. (2011). We also reported the presence of 15 X-ray galaxy clusters

Table 5
X-Ray Emission from Radio Extended Structures (i.e., Knots and Hotspots)

3CR Name	Component	Class	Counts	$F_{0.5-1\,keV}$[a] (cgs)	$F_{1-2\,keV}$[a] (cgs)	$F_{2-7\,keV}$[a] (cgs)	$F_{0.5-7\,keV}$[a] (cgs)	L_X (10^{42} erg s^{-1})
13.0	n16.5	h	5 (0.375)	0.58 (0.34)	0.16 (0.16)	0.76 (0.76)	1.5 (0.85)	18.27 (10.35)
65.0	e6.6	h	4 (0.375)	0.23 (0.23)	0.0 (0.0)	1.01 (1.01)	1.24 (1.04)	10.68 (8.95)
65.0	w6.7	h	7 (0.25)	0.46 (0.27)	0.4 (0.29)	0.72 (0.72)	1.58 (0.82)	13.6 (7.06)
68.2	n11.5	h	5 (0.25)	0.0 (0.0)	1.02 (0.46)	0.0 (0.0)	1.02 (0.46)	18.21 (8.21)
78.0	e1.6	k	1001 (406)	15.58 (1.29)	22.46 (1.61)	39.19 (3.84)	77.22 (4.36)	0.15 (0.01)
88.0	e109	k	33 (6.75)	0.71 (0.26)	0.77 (0.25)	0.72 (1.02)	2.2 (1.08)	0.005 (0.002)
181.0	e4.5	h	3 (0.125)	1.21 (1.21)	0.94 (0.94)	2.7 (2.7)	4.86 (3.11)	62.64 (40.08)
191.0	s1.9[b]	k	18 (0.125)	1.01 (0.42)	0.86 (0.44)	3.19 (1.6)	5.07 (1.71)	154.99 (52.28)
200.0	s9.3[b]	k	6 (0.125)	0.0 (0.0)	0.7 (0.41)	1.49 (1.49)	2.19 (1.54)	1.84 (1.3)
210.0	s7.6	h	5 (0.125)	0.28 (0.2)	0.28 (0.28)	0.65 (0.65)	1.21 (0.74)	10.26 (6.28)
215.0	e2.6[b]	k	26 (0.25)	0.31 (0.28)	0.14 (0.36)	1.06 (1.12)	1.5 (1.21)	0.97 (0.79)
228.0	n24.8	h	6 (0.125)	0.0 (0.0)	1.03 (0.46)	0.59 (0.59)	1.62 (0.75)	2.14 (0.99)
228.0	s21.4	h	16 (0.125)	1.35 (0.48)	2.25 (0.8)	0.0 (0.0)	3.6 (0.93)	4.76 (1.23)
245.0	w1.5[b]	k	26 (0.125)	1.98 (0.76)	0.76 (1.07)	1.16 (2.32)	3.9 (2.66)	24.05 (16.4)
268.1	w25	h	25 (0.125)	0.71 (0.5)	5.95 (1.49)	11.08 (4.19)	17.74 (4.47)	95.13 (23.97)
299.0	e2.7	h	22 (0.375)	0.94 (0.28)	1.0 (0.32)	0.45 (0.45)	2.39 (0.62)	1.19 (0.31)
324.0	e5.8	h	9 (0.5)	0.18 (0.1)	0.23 (0.12)	0.42 (0.42)	0.84 (0.45)	7.7 (4.13)
325.0	e6.8	h	10 (0.375)	0.34 (0.19)	0.34 (0.25)	0.95 (0.68)	1.63 (0.75)	6.43 (2.96)
325.0	w9.2	h	7 (0.125)	0.1 (0.1)	0.21 (0.21)	1.73 (0.86)	2.03 (0.89)	8.0 (3.51)
334.0	s2.7[b]	k	30 (0.625)	1.0 (0.32)	0.94 (0.4)	0.25 (0.81)	2.19 (0.95)	2.93 (1.27)
334.0	s17.5[b]	k	26 (5.75)	0.76 (0.27)	1.1 (0.37)	1.99 (1.82)	3.85 (1.87)	5.15 (2.5)
437.0	n19	h	12 (0.625)	0.48 (0.28)	0.74 (0.37)	3.32 (1.66)	4.54 (1.72)	69.43 (26.3)
437.0	s17	h	7 (0.5)	0.32 (0.23)	0.22 (0.22)	1.28 (1.19)	1.83 (1.24)	27.98 (18.96)
470.0	n14.4	h	1 (0.75)	0.0 (0.0)	0.0 (0.0)	0.29 (0.66)	0.29 (0.66)	5.84 (13.29)
470.0	s9.4	h	10 (0.625)	0.76 (0.38)	0.33 (0.24)	2.0 (1.42)	3.1 (1.49)	62.43 (30.01)

Notes. Col. (1): the 3CR name. Col. (2): the component name chosen according to the definition reported in Section 4.2. Col. (3): the component class: "h"= hotspot; "k"= knot. Col. (4): the number of counts column gives the total counts in the photometric circle, together with the average of the eight background regions, in parentheses; both for the 0.5–7 keV band. Col. (5): measured X-ray flux between 0.5 and 1 keV. Col. (6): measured X-ray flux between 1 and 2 keV. Col. (7): measured X-ray flux between 2 and 7 keV. Col. (8): measured X-ray flux between 0.5 and 7 keV. Col. (9): X-ray luminosity in the range 0.5–7 keV, with the 1σ uncertainties given in parentheses.

[a] Source components for which the X-ray emission was already reported in the literature.

[b] Fluxes are given in units of 10^{-15} erg cm^{-2} s^{-1}, and 1σ uncertainties are given in parentheses. The uncertainties on the flux measurements were computed as described in Section 4.2.

Table 6
X-Ray Galaxy Clusters

3CR Name	Other Name	z	R (arcsec)	R (kpc)	Total Counts
28.0	Abell 115	0.195	200	632	31450
40.0	Abell 194	0.0181	170	60	23855
75.0	Abell 400	0.023	500	228	57400
88.0	1RXS J032755.0+023403	0.0302	120	70	6610
220.1	1RXS J093245.5+790636	0.61	25	166	1722
288.0	1RXS J133849.3+385110	0.246	60	680	5324
310.0	SDSS J150457.12+260058.4	0.0538	180	183	28309
318.1	Abell 2063B	0.0453	500	433	272770
338.0	Abell 2199	0.03035	500	296	504360
388.0	1RXS J184402.1+453332	0.0917	240	400	15416
401.0	1RXS J194024.4+604136	0.055	90	292	3200
427.1	⋯	0.572	40	257	467
438.0	1RXS J215553.4+380021	0.290	210	894	66288
442.0	1RXS J221451.0+135040	0.0263	300	155	15506
449.0	⋯	0.017	240	81	42378

Note. Col. (1): the 3CR name. Col. (2): alternative name. Col. (3): the source redshift. Col. (4): radius in arcseconds. Col. (5): radius in kiloparsecs. Col. (6): the net counts.

Table 7
Image Parameters

3CR Name	Radio Freq. (GHz)	HPBW (radio)-(arcsec × arcsec)	Low-contour-level (radio)-(mJy/beam)	Factor Increase (radio)	NRAO Project Code	Binning Factor (X-rays)	FWHM-smoothing (X-rays)-(arcsec)
2[a]	1.5	1.2 × 1.4	6.4	4	AH0171–(NVAS)	1/4	0.72
13.0	4.9	0.37	1.0	2	AC0200–(NVAS)	1/8	0.51
14.0	8.5	0.23	3.0	4	AL0280–(NVAS)	1/8	0.51
22.0	8.5	0.25	0.125	4	AP380–(MJH)	1/8	0.51
28.0	1.4	1.10	0.25	4	AL272–(NED)	1/8	0.65
35.0	1.5	17 × 14	4.0	2	AW0087–(NVAS)	1	4.0
40.0	1.6	23 × 12	4.0	4	AB0022–(NVAS)	2	8.0
43.0	8.3	0.23	6.0	4	AJ0206–(NVAS)	1/8	0.51
48.0	4.8	0.59 × 0.47	12.5	4	AW0227–(NVAS)	1/8	0.36
49.0	4.9	0.41	4.0	4	NEFF–(NED)	1/8	0.36
65.0	1.5	1.28 × 1.13	4.0	2	PERL–(NVAS)	1/8	0.51
68.1	1.4	1.46 × 1.33	2.0	2	AW0482–(NVAS)	1/4	1.0
68.2	4.9	0.53 × 0.39	1.0	2	AV0164–(NVAS)	1/4	0.72
75.0	4.6	4.6 × 3.8	0.25	4	AE0061–(NVAS)	1	1.7
78.0[b]	1.5	4.3 × 3.9	2.0	2	AB0376–(NVAS)	1/8	0.51
88.0	4.9	4.4 × 4.2	1.0	2	AP0077–(NVAS)	1/2	1.4
98.0	8.3	2.0	0.25	2	PERL–(NED)	1	4.0
99.0	4.8	0.45 × 0.39	1.0	4	AS302–(NVAS)	1/4	5.0
129.1	4.8	1.25	0.125	2	AT229–(NVAS)	1/4	1.0
136.1	1.6	3.3	2.0	2	POOL–(NVAS)	1	3.5
138.0	4.9	0.42	1.0	4	AL0142–(NVAS)	1/8	0.51
147.0	8.4	0.27	19.2	4	AK403–(CCC)	1/8	0.36
172.0	8.5	0.90	0.125	4	AP361–(MJH)	1/4	0.72
175.0	8.5	0.78 × 0.61	0.5	4	AH0452–(NVAS)	1/4	0.72
175.1	4.9	0.35	1.2	4	AP380–(MJH)	1/8	0.36
181.0	4.9	0.37	1.0	4	AH0552–(NVAS)	1/8	0.36
184.0	8.5	0.36 × 0.20	16.0	4	AK0403–(NVAS)	1/8	0.36
190.0	8.5	0.20	4.0	2	AO0105–(NVAS)	1/8	0.36
191.0	4.7	0.30	0.3	4	AK180–(CCC)	1/8	0.36
192.0	8.2	0.80	0.125	4	PERL–(NED)	1/2	1.4
196.0	4.9	0.35	0.5	4	AB516–(MJH)	1/8	0.36
200.0	8.5	0.25	0.125	4	AP331–(MJH)	1/8	0.65
204.0	8.3	0.78 × 0.65	0.5	4	AW0249–(NVAS)	1/8	0.51
205.0	8.3	0.22	2.0	4	AW0330–(NVAS)	1/8	0.36
208.0	8.4	0.25	0.125	4	AL280–(CCC)	1/8	0.36
210.0	1.4	1.6	6.4	4	AO230–(TW)	1/4	1.3
215.0[c]	4.9	0.37	0.1	4	BRID–(MJH)	1/8	0.36
216.0	8.2	0.25	4.8	4	AG357–(MJH)	1/8	0.36
220.1	8.4	0.25	0.1	4	AP380–(MJH)	1/8	0.36
220.3[d]	8.4	0.70 × 0.43	1.0	2	AM0384–(NVAS)	1/8	0.51
226.0	8.5	0.20	0.125	4	AP380–(MJH)	1/8	0.51
228.0	8.5	0.23	0.125	4	AP331–(MJH)	1/8	0.51
241.0	8.4	0.20	1.2	4	AA0149–(NVAS)	1/8	0.36
245.0	4.9	0.25	0.5	4	AB244–(CCC)	1/8	0.36
249.1	4.9	0.35	0.1	4	BRID–(MJH)	1/8	0.36
252.0	4.9	1.0	0.5	4	AF0213–(NVAS)	1/4	1.0
256.0	4.8	1.7 × 1.4	0.4	4	AM244–(TW)	1/4	1.0
263.1	4.9	0.35	0.25	4	DREH–(MJH)	1/8	0.36
266.0	8.4	0.30	0.4	4	AK403–(CCC)	1/8	0.51
267[e]	8.4	0.85 × 0.74	0.125	4	AL330–(TW)	1/8	0.36
268.1	8.5	0.25	0.25	4	AP380–(MJH)	1/8	0.51
268.3	5.0	0.06	1.2	4	MERLIN2–(MJH)	1/16	0.33
268.4	8.3	0.72 × 0.58	2.0	4	AW0249–(NVAS)	1/8	0.36
270.1	4.9	0.36	4.8	4	AB0522–(NVAS)	1/8	0.51
277.1	22.5	0.09	1.0	4	AV231–(TW)	1/8	0.36
277.3	4.9	0.37	1.0	2	CORD–(NVAS)	1/8	0.36
285.0	1.5	1.2	0.3	4	AV0127–(NVAS)	1/4	0.72
286.0	8.0	0.28 × 0.23	4.8	4	AG0357–(NVAS)	1/8	0.36
287.0	8.5	0.24	10.0	4	AK0276–(NVAS)	1/16	0.18
288.0	4.9	0.6	0.5	4	ED–(NED)	1/4	1.3
289.0	5.0	0.06	0.4	4	MERLIN2–(MJH)	1/8	0.51

Table 7
(Continued)

3CR Name	Radio Freq. (GHz)	HPBW (radio)-(arcsec × arcsec)	Low-contour-level (radio)-(mJy/beam)	Factor Increase (radio)	NRAO Project Code	Binning Factor (X-rays)	FWHM-smoothing (X-rays)-(arcsec)
298.0	8.3	0.25	10.0	4	AJ0206–(NVAS)	1/16	0.18
299.0	1.5	0.13	1.0	4	MERLIN2–(NED)	1/8	0.36
309.1	14.9	0.17 × 0.11	4.0	4	TESTT–(NVAS)	1/8	0.36
310.0	1.5	15 × 12	10.0	2	AB0182–(NVAS)	1	7.5
318.0	8.5	0.22	20.0	2	AA0149–(NVAS)	1/8	0.51
318.1	1.4	4.7 × 4.4	0.3	4	FOMA–(NVAS)	1/2	2.0
324.0	4.9	0.38	0.125	4	AF186–(CCC)	1/8	0.36
325.0	4.9	0.35	0.5	4	AF213–(MJH)	1/8	0.51
334.0	4.9	0.35	0.125	4	BRID–(MJH)	1/8	0.51
336.0	4.9	0.35	0.1	4	AB454–(MJH)	1/4	0.72
337.0	4.9	0.40	0.25	4	AP114–(MJH)	1/4	1.0
338.0	4.9	1.0	0.1	2	AG269–(NED)	1/4	0.72
340.0	4.9	0.40	0.125	4	AP380–(MJH)	1/4	1.0
343.0	4.9	0.42	19.2	4	AB0922–(NVAS)	1/4	0.72
343.1	1.5	1.3	32.0	4	AM0178–(NVAS)	1/8	0.51
352.0	4.7	0.35	0.25	4	AG247–(MJH)	1/8	0.36
356.0	4.9	0.45 × 0.38	0.75	4	AF0186–(NVAS)	1/4	0.72
368.0	8.5	0.2	0.3	4	AL0322–(NVAS)	1/4	0.72
382.0	8.4	0.75	0.125	4	PERL–(NED)	1/4	0.72
388.0	4.9	0.47 × 0.36	0.25	4	AC0149–(NVAS)	1/8	0.94
401.0	8.4	0.27	0.1	4	AP315–(MJH)	1/8	0.51
(401b)	8.4	0.27	0.1	4	AP315–(MJH)	1/2	3.8
427.1	8.5	0.25	0.1	4	AP331–(MJH)	1/4	0.72
(427.1b)	8.5	0.25	0.1	4	AP331–(MJH)	1/2	3.8
432.0	4.9	0.40	2.0	2	AB0454–(NVAS)	1/8	0.51
433.0	8.5	0.25	0.1	2	AB534–(MJH)	1/4	0.72
437.0	4.9	1.2	4.0	4	AV164–(TW)	1/4	1.0
438.0	8.4	0.23	0.125	4	AP315–(NED)	1/4	1.3
441.0	4.9	0.35	0.25	4	AF213–(MJH)	1/8	0.51
442.0	1.4	7.5	0.5	2	PEGG–(NED)	2	5.8
449.0	1.5	4.0	0.125	4	AK319–(CCC)	2	8.1
(Insert)	1.7	1.2	0.25	4	PERL–(NVAS)	1/2	1.4
455.0	4.9	0.40	0.5	4	AP331–(MJH)	1/8	0.51
469.1	4.9	1.7 × 1.1	2.0	4	AR0123–(NVAS)	1/4	0.72
470.0	8.4	1.5 × 1.3	2.0	4	AL330–(TW)	1/4	0.72

Notes. Col. (1): the 3CR name. Col. (2): the binning factor of the X-ray image (see Section 4.2 for more details). Col. (3): the FWHM of the smoothing kernel chosen for the X-ray image. Col. (4): the value of the lowest contour level of the radio map overlaid to the X-ray image. Col. (5): the factor increase of the radio contours. Col. (6): the radio frequency of the radio map used for the comparison with the X-ray image. Col. (7): the half-power beam width (HPBW) of the reduced radio images. Single numbers are reported for circular beam. Col. (8): the identification number of the observer program, as reported in the header of the raw *u*,*v* data downloaded from the VLA archive (see https://archive.nrao.edu/archive/nraodashelpj.html for more details).

[a] 3CR 2 is 7.′9 off axis, so we did not register the X-ray image. The source appears to be extended in the X-rays (~8″), but since it is so far off axis, the apparent size is consistent with the *Chandra* point-spread function.

[b] The white contours at the nucleus are from a Merlin observation, performed at 1.4 GHz on 1998 May 5, showing the small-scale jet. The X-ray images come from a 1/8 subarray observation, and the width of the subarray is smaller than the size of the radio source. The readout streak is evident and lies, unfortunately, along the direction of the jet and the primary axis of the radio emission.

[c] The prominent readout streak goes right through the jet segment superposed on the *E* lobe.

[d] This is a radio galaxy lying at $z = 0.685$, which is lensing a submillimeter galaxy at $z = 2.221$ (Haas et al. 2014).

[e] There may be a wcs problem with the coordinates of the radio image of the order of 1″, and so the R.A./decl. labels could be slightly off.

associated with the selected 3CR source, all already known in the X-rays.

In the appendices, we present X-ray images with radio contours for all 93 sources analyzed in this paper (Appendix A) and give the *Chandra* status of the observations for all extragalactic 3CR sources (Appendix B).

We thank the anonymous referee for useful comments that led to improvements in the paper. We are grateful to M. Hardcastle and C. C. Cheung for providing several radio images of the 3CR sources, while the remaining ones were downloaded from the NVAS[14] (NRAO VLA Archive Survey), NED[15] (Nasa Extragalactic Database), and the DRAGN webpage.[16] This investigation is supported by the NASA grants GO1-12125A, GO2-13115X, and GO4-15097X. G.R.T acknowledges support by the European Community's Seventh

[14] http://archive.nrao.edu/nvas/

[15] http://ned.ipac.caltech.edu/

[16] http://www.jb.man.ac.uk/atlas/

Table 8
The Current Status of the 3CR *Chandra* Observations

3CR Name	Class	z	D_L (Mpc)	Cluster Flag	X-Ray Detection	*Chandra* Flag
2.0	QSR	1.037367	7252.26	no	⋯	yes
6.1	FRII	0.8404	5577.63	no	h	yes
9.0	QSR	2.019922	16632.24	no	k, l	yes
11.1	UND	?	⋯	no	⋯	no
13.0	FRII	1.351	10088.93	no	h	yes
14.0	QSR	1.469	11200.31	no	⋯	yes
14.1	UND	?	⋯	no	⋯	no
15.0	FRI	0.073384	341.93	no	k, l	yes
16.0	FRII	0.405	2288.92	no	h, l	yes
17.0	QSR	0.219685	1126.33	no	k	yes
18.0	FRII	0.188	945.54	no	⋯	yes
19.0	FRII	0.482	2819.56	yes	h	yes
20.0	FRII	0.174	867.55	no	⋯	yes
21.1	UND	?	⋯	no	⋯	no
22.0	FRII	0.936	6378.57	no	⋯	yes
27.0	FRII	0.184	923.17	no	⋯	no
28.0	FRI	0.195275	986.54	yes	xcl	yes
29.0	FRI	0.045031	205.48	yes	k	yes
31.0	FRI	0.017005	75.94	yes	k	yes
33.0	FRII	0.0597	275.49	no	h	yes
33.1	FRII	0.180992	906.44	no	⋯	yes
33.2	UND	?	⋯	no	⋯	no
34.0	FRII	0.69	4368.53	no	⋯	yes
35.0	FRII	0.067013	310.8	no	⋯	yes
36.0	QSR	1.301	9624.8	no	⋯	no
40.0	FRII	0.018	80.46	yes	xcl	yes
41.0	FRII	0.795	5205.64	no	⋯	yes
42.0	FRII	0.395007	2221.96	no	⋯	yes
43.0	QSR	1.459	11105.41	no	⋯	yes
44.0	FRII	0.66	4135.83	yes	⋯	yes
46.0	FRII	0.4373	2508.42	yes	⋯	yes
47.0	QSR	0.425	2424.27	no	h, l	yes
48.0	QSR	0.367	2036.73	no	⋯	yes
49.0	FRII	0.621	3837.6	no	⋯	yes
52.0	FRII	0.29	1546.9	yes	h	yes
54.0	FRII	0.8274	5470.44	no	⋯	yes
55.0	FRII	0.7348	4721.63	no	⋯	yes
63.0	FRII	0.175	873.1	no	⋯	yes
61.1	FRII	0.18781	944.47	no	h	yes
65.0	FRII	1.176	8483.18	no	h	yes
66.0A	BL	?	⋯	yes	⋯	yes
66.0B	FRI	0.021258	95.28	yes	k	yes
67.0	FRII	0.3102	1672.55	no	⋯	yes
68.1	QSR	1.238	9045.91	no	⋯	yes
68.2	FRII	1.575	12216.2	no	h	yes
69.0	FRII	0.458	2651.47	no	⋯	no
71.0	Sy	0.003793	16.72	no	⋯	yes
75.0	FRI	0.023153	103.9	yes	xcl	yes
76.1	FRII	0.032489	146.82	no	⋯	yes
78.0	FRI	0.028653	129.09	no	k	yes
79.0	FRII	0.255900	1339.62	yes	⋯	yes
83.1	FRI	0.025137	112.95	yes	k, xcl	yes
84.0	FRI	0.017559	78.45	yes	xcl	yes
86.0	FRII	?	⋯	no	⋯	no
88.0	FRI	0.030221	136.32	yes	k, xcl	yes
89.0	FRI	0.1386	675.57	yes	xcl	yes
91.0	UND	?	⋯	no	⋯	no
93.0	QSR	0.35712	1972.32	no	⋯	yes
93.1	FRII	0.243	1262.81	yes	⋯	yes
98.0	FRII	0.030454	137.4	no	⋯	yes
99.0	Sy	0.426	2431.07	yes	⋯	yes
103.0	FRII	0.33	1797.71	no	⋯	yes
105.0	FRII	0.089	419.33	no	k, h	yes

Table 8
(Continued)

3CR Name	Class	z	D_L (Mpc)	Cluster Flag	X-Ray Detection	*Chandra* Flag
107.0	FRII	0.785	5124.51	no	⋯	yes
109.0	FRII	0.3056	1643.78	no	h, l	yes
111.0	FRII	0.0485	221.87	no	k, h	yes
114.0	FRII	0.815	5368.77	no	⋯	yes
119.0	FRII	1.023	7127.0	no	⋯	no
123.0	FRII	0.2177	1114.8	yes	k	yes
124.0	FRII	1.083	7653.06	no	⋯	no
125.0	UND	?	⋯	no	⋯	no
129.0	FRI	0.0208	93.2	yes	k, xcl	yes
129.1	FRI	0.0222	99.56	no	⋯	yes
130.0	FRI	0.109	520.76	no	⋯	yes
131.0	UND	?	⋯	no	⋯	no
132.0	FRII	0.214	1093.4	yes	⋯	yes
133.0	FRII	0.2775	1470.27	no	⋯	yes
134.0	UND	?	⋯	no	⋯	no
135.0	FRII	0.12738	616.21	yes	⋯	yes
136.1	FRII	0.064	296.2	no	⋯	yes
137.0	UND	?	⋯	no	⋯	no
138.0	QSR	0.759	4915.0	no	⋯	yes
139.2	FRII	?	⋯	no	⋯	no
141.0	UND	?	⋯	no	⋯	no
142.1	FRII	0.4061	2296.3	no	⋯	yes
147.0	QSR	0.545	3271.83	no	⋯	yes
152.0	UND	?	⋯	no	⋯	no
153.0	FRII	0.2769	1466.59	yes	⋯	yes
154.0	QSR	0.58	3529.84	no	⋯	yes
158.0	UND	?	⋯	no	⋯	no
165.0	FRII	0.2957	1582.19	no	⋯	yes
166.0	FRII	0.2449	1274.04	no	⋯	yes
169.1	FRII	0.633	3928.69	no	⋯	yes
171.0	FRII	0.2384	1235.67	no	⋯	yes
172.0	FRII	0.5191	3084.06	no	⋯	yes
173.0	QSR	1.035	7231.55	no	⋯	no
173.1	FRII	0.2921	1559.87	yes	h, l	yes
175.0	QSR	0.77	5003.31	no	⋯	yes
175.1	FRII	0.92	6242.98	no	⋯	yes
180.0	FRII	0.22	1128.16	no	⋯	yes
181.0	QSR	1.382	10378.89	no	h	yes
184.0	FRII	0.994	6875.53	no	⋯	yes
184.1	FRII	0.1182	568.34	yes	⋯	yes
186.0	QSR	1.068634	7526.33	yes	xcl	yes
187.0	FRII	0.465	2700.19	no	l	yes
190.0	QSR	1.195649	8660.73	no	⋯	yes
191.0	QSR	1.956	15984.33	no	k, l	yes
192.0	FRII	0.059709	275.53	yes	⋯	yes
194.0	FRII	1.184	8555.38	no	⋯	no
196.0	QSR	0.871	5831.32	no	⋯	yes
196.1	FRII	0.198	1002.01	no	⋯	yes
197.1	FRII	0.128009	619.51	yes	⋯	yes
198.0	FRII	0.081474	381.9	yes	⋯	yes
200.0	FRII	0.458	2651.47	yes	k, l	yes
204.0	QSR	1.112	7909.99	no	⋯	yes
205.0	QSR	1.534	11821.39	no	⋯	yes
207.0	QSR	0.6808	4296.94	no	k, l	yes
208.0	QSR	1.111510	7905.63	no	⋯	yes
208.1	QSR	1.02	7100.98	no	⋯	no
210.0	FRII	1.169	8420.05	no	h	yes
212.0	QSR	1.048	7345.18	no	h	yes
213.1	FRI	0.19392	978.87	yes	h	yes
215.0	QSR	0.4121	2336.74	no	k, l	yes
217.0	FRII	0.8975	6053.2	no	⋯	yes
216.0	QSR	0.669915	4212.31	no	⋯	yes

Table 8
(Continued)

3CR Name	Class	z	D_L (Mpc)	Cluster Flag	X-Ray Detection	*Chandra* Flag
219.0	FRII	0.174732	871.61	yes	k, l	yes
220.1	FRII	0.61	3754.31	yes	xcl	yes
220.2	QSR	1.157429	8316.07	no	⋯	no
220.3	FRII	0.68	4290.73	no	⋯	yes
222.0	FRI	1.339	9977.24	no	⋯	no
223.0	FRII	0.13673	665.6	yes	⋯	yes
223.1	FRII	0.107474	512.94	no	⋯	yes
225.0A	FRII	1.565	12119.69	no	⋯	yes
225.0B	FRII	0.58	3529.84	no	⋯	yes
226.0	FRII	0.8177	5390.92	no	⋯	yes
227.0	FRII	0.086272	405.71	no	h	yes
228.0	FRII	0.5524	3325.95	no	h	yes
230.0	FRII	1.487	11371.7	no	⋯	no
231.0	FRI	0.000677	2.97	no	⋯	yes
234.0	FRII	0.184925	928.33	no	h	yes
236.0	FRII	0.1005	477.44	no	⋯	yes
237.0	FRII	0.877	5881.45	no	⋯	yes
238.0	FRII	1.405	10594.89	no	⋯	no
239.0	FRII	1.781	14232.66	no	⋯	no
241.0	FRII	1.617	12622.99	no	⋯	yes
244.1	FRII	0.428	2444.69	yes	⋯	yes
245.0	QSR	1.027872	7169.36	no	k	yes
247.0	FRII	0.7489	4834.0	yes	⋯	yes
249.0	QSR	1.554	12013.69	no	⋯	no
249.1	QSR	0.3115	1680.71	no	⋯	yes
250.0	FRII	?	⋯	no	⋯	no
252.0	FRII	1.1	7803.57	no	⋯	yes
254.0	QSR	0.736619	4736.12	no	h	yes
255.0	QSR	1.355	10126.27	no	⋯	no
256.0	FRII	1.819	14610.18	no	⋯	yes
257.0	QSR	2.474	21340.67	no	⋯	no
258.0	FRI	0.165	818.03	yes	⋯	yes
263.0	QSR	0.646	4028.06	no	h	yes
263.1	FRII	0.824	5442.55	no	⋯	yes
264.0	FRI	0.021718	97.37	yes	k	yes
265.0	FRII	0.811	5336.02	no	h, l	yes
266.0	FRII	1.275	9384.99	no	⋯	yes
267.0	FRII	1.14	8159.88	no	⋯	yes
268.1	FRII	0.97	6668.89	no	h	yes
268.2	FRII	0.362	2004.12	yes	h	yes
268.3	FRII	0.37171	2067.61	no		yes
268.4	QSR	1.402200	10568.59	no	⋯	yes
270.0	FRI	0.007378	32.63	yes	k	yes
270.1	QSR	1.528432	11767.94	no	⋯	yes
272.0	FRII	0.944	6446.64	no	⋯	yes
272.1	FRI	0.003392	14.94	yes	k	yes
273.0	QSR	0.158339	781.73	no	k	yes
274.0	FRI	0.004283	18.89	yes	k, xcl	yes
274.1	FRII	0.422	2403.91	no	⋯	yes
275.0	FRII	0.48	2805.51	yes	⋯	yes
275.1	QSR	0.5551	3345.78	no	k, h, l	yes
277.0	FRI	0.414	2349.59	no	⋯	yes
277.1	QSR	0.31978	1732.99	no		yes
277.2	FRII	0.766	4971.13	no	⋯	yes
277.3	FRII	0.085336	401.05	no	⋯	yes
280.0	FRII	0.996	6892.84	yes	k, h, l	yes
280.1	QSR	1.667065	13110.8	no	l	no
284.0	FRII	0.239754	1243.68	yes	⋯	yes
285.0	FRII	0.0794	371.64	no	⋯	yes
286.0	QSR	0.849934	5656.31	no	⋯	yes
287.0	QSR	1.055	7406.56	no	⋯	yes
287.1	FRII	0.215567	1102.45	no	h	yes
288.0	FRI	0.246	1280.56	yes	xcl	yes
288.1	QSR	0.96296	6608.61	no	⋯	yes
289.0	FRII	0.9674	6646.6	no	⋯	yes
292.0	FRII	0.71	4525.37	no	⋯	yes
293.0	FRI	0.045034	205.5	no	⋯	yes
293.1	FRII	0.709	4517.5	no	⋯	yes
294.0	FRII	1.779	14212.84	yes	h, xcl	yes
295.0	FRII	0.4641	2693.92	yes	h, xcl	yes
296.0	FRI	0.024704	110.97	no	k	yes
297.0	QSR	1.4061	10605.23	no	⋯	no
298.0	QSR	1.438120	10907.49	no		yes
299.0	FRII	0.367	2036.73	yes	h	yes
300.0	FRII	0.27	1424.56	no	⋯	yes
300.1	FRII	1.15885	8328.86	no	⋯	no
303.0	FRI	0.141186	689.35	yes	k	yes
303.1	FRI	0.2704	1426.99	no	⋯	yes
305.0	FRII	0.041639	189.56	no	⋯	yes
305.1	FRII	1.132	8088.23	no	⋯	no
306.1	FRII	0.441	2533.89	yes	⋯	yes
309.1	QSR	0.905	6116.25	no	⋯	yes
310.0	FRI	0.0538	247.11	yes	xcl	yes
314.1	FRI	0.1197	576.16	yes	⋯	yes
313.0	FRII	0.461000	2672.37	yes	h, xcl	yes
315.0	FRI	0.1083	517.17	yes	⋯	yes
317.0	FRI	0.034457	155.96	yes	xcl	yes
318.0	FRII	1.574	12206.53	yes	⋯	yes
318.1	FRI	0.045311	206.8	yes	xcl	yes
319.0	FRII	0.192	968.03	yes	⋯	yes
320.0	FRII	0.342	1874.59	yes	xcl	yes
321.0	FRII	0.0961	455.08	no	h	yes
322.0	FRII	1.681	13247.25	no	⋯	no
323.0	FRII	0.679	4282.93	no	⋯	yes
323.1	QSR	0.2643	1390.12	yes	⋯	yes
324.0	FRII	1.2063	8757.25	yes	h	yes
325.0	FRII	1.135	8115.06	no	h	yes
326.0	FRII	0.0895	421.83	no	⋯	yes
326.1	FRII	1.825	14669.88	no	⋯	no
327.0	FRII	0.1048	499.28	yes	h	yes
327.1	FRI	0.462	2679.32	no	k	yes
330.0	FRII	0.55	3308.36	yes	h	yes
332.0	FRII	0.151019	742.01	yes	⋯	yes
334.0	QSR	0.5551	3345.78	no	k, l	yes
336.0	QSR	0.926542	6298.25	no	⋯	yes
337.0	FRII	0.635	3943.96	yes	⋯	yes
338.0	FRI	0.030354	136.94	yes	xcl	yes
340.0	FRII	0.7754	5046.9	no	⋯	yes
341.0	FRII	0.448	2582.06	no	k	yes
343.0	QSR	0.988	6823.74	no	⋯	yes
343.1	FRII	0.75	4842.79	no	⋯	yes
345.0	QSR	0.5928	3625.15	no	k	yes
346.0	FRI	0.162012	801.73	yes	k	yes
348.0	FRI	0.155	763.55	yes	xcl	yes
349.0	FRII	0.205	1041.79	no	h	yes
351.0	FRII	0.37194	2069.13	no	h	yes
352.0	FRII	0.8067	5300.91	no	⋯	yes
353.0	FRII	0.030421	137.25	no	k	yes
356.0	FRII	1.079	7617.8	no	⋯	yes
357.0	FRII	0.166148	824.31	yes	⋯	yes
368.0	FRII	1.131	8079.29	no		yes
371.0	BL	0.051	233.74	no	k	yes
379.1	FRII	0.256	1340.22	no	⋯	yes
380.0	QSR	0.692	4384.16	no	k	yes

Table 8
(Continued)

3CR Name	Class	z	D_L (Mpc)	Cluster Flag	X-Ray Detection	*Chandra* Flag
381.0	FRII	0.1605	793.51	no	⋯	yes
382.0	FRII	0.05787	266.65	no	⋯	yes
386.0	FRI	0.016885	75.39	no	⋯	yes
388.0	FRII	0.0917	432.88	yes	xcl	yes
389.0	UND	?	⋯	no	⋯	no
390.0	UND	?	⋯	no	⋯	no
390.3	FRII	0.0561	258.14	no	k, h	yes
394.0	UND	?	⋯	no	⋯	no
399.1	FRII	?	⋯	no	⋯	no
401.0	FRII	0.2011	1019.64	yes	xcl	yes
402.0	FRI	0.025948	116.67	yes	k	yes
403.0	FRII	0.059	272.1	no	k, h	yes
403.1	FRII	0.0554	254.77	yes	⋯	yes
405.0	FRII	0.056075	258.01	yes	h, xcl	yes
409.0	FRII	?	⋯	no	⋯	no
410.0	FRII	0.2485	1295.4	no	⋯	yes
411.0	FRII	0.467	2714.14	no	⋯	yes
415.2	UND	?	⋯	no	⋯	no
418.0	QSR	1.686	13296.15	no	⋯	no
424.0	FRI	0.126988	614.15	yes	⋯	yes
427.1	FRII	0.572	3470.35	yes	l,xcl	yes
428.0	UND	?	⋯	no	⋯	no
430.0	FRII	0.055545	255.47	yes	⋯	yes
431.0	UND	?	⋯	no	⋯	no
432.0	QSR	1.785	14272.26	no	⋯	yes
434.0	FRII	0.322	1746.99	yes	⋯	yes
433.0	FRI	0.1016	483.01	no	⋯	yes
435.0	FRII	0.471	2742.13	no	⋯	yes
436.0	FRII	0.2145	1096.28	no	h	yes
437.0	FRII	1.48	11305.11	no	h	yes
438.0	FRII	0.29	1546.9	yes	xcl	yes
441.0	FRII	0.708	4509.63	no	⋯	yes
442.0	FRI	0.0263	118.28	yes	xcl	yes
445.0	FRII	0.055879	257.07	yes	h	yes
449.0	FRI	0.017085	76.3	yes	xcl	yes
452.0	FRII	0.081100	380.05	no	h, l	yes
454.0	QSR	1.757	13995.04	no	⋯	no
454.1	FRII	1.841	14829.49	yes	⋯	no
454.2	UND	?	⋯	no	⋯	no
454.3	QSR	0.859	5731.6	no	k	yes
455.0	QSR	0.543	3257.27	no	⋯	yes
456.0	FRII	0.233	1203.84	no	⋯	yes
458.0	FRII	0.289	1540.74	yes	h	yes
459.0	FRII	0.22012	1128.85	no	l	yes
460.0	FRII	0.268	1412.45	yes	⋯	yes
465.0	FRI	0.030221	136.32	yes	k, xcl	yes
468.1	UND	?	⋯	no	⋯	no
469.1	FRII	1.336	9949.27	no	⋯	yes
470.0	FRII	1.653	12973.42	no	h	yes

Note. Col. (1): the 3CR name. Col. (2): the radio-to-optical classification of the sources: FRI and FRII refer to the Fanaroff and Riley classification criterion for radio galaxies (Fanaroff & Riley 1974); QSR stands for quasars; Sy for Seyfert galaxies; and BL for BL Lac objects. We used the acronym UND for sources that are still unidentified, i.e., lacking an optical spectroscopic observation. Col. (3): redshift z. We also verified in the literature (e.g., NED and/or SIMBAD databases) whether new z values were reported after the release of the 3CR catalog. Col. (4): luminosity distance in Mpc. Cosmological parameters used to compute it are reported in Section 1. Col. (5): the "cluster flag" indicates if the source is known to be associated with a cataloged cluster of galaxies or if there is significantly extended X-ray emission around the host galaxy, i.e., on scales of 100 kpc or greater. Col. (6): in this column we report whether the source has a radio component with an X-ray counterpart. We used the following labels: k = jet knot; h = hotspot; l = lobe. We also indicated xcl if there is a galaxy cluster detected in the X-rays. Col. (7): the "*Chandra* flag" indicates if the source was already observed by *Chandra*. Question marks in the redshift column (i.e., col. 3) indicate that no optical spectra are present in the literature at the best of our knowledge and thus no z estimate was found.

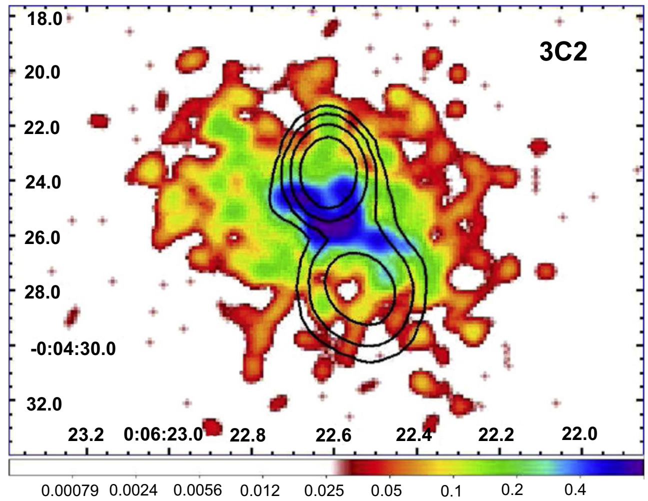

Figure 1. X-ray image corresponding to the Chandra observation (Table 2) with contours of radio brightness superposed. The image is re-binned to change the pixel size and is smoothed with a Gaussian function. The underlying color bar shows the X-ray brightness in units of counts per pixel. Radio contours are logarithmically spaced. All relevant parameters for each source are given in Table 7.

(The complete figure set (95 images) is available.)

Framework Programme (/FP7/2007-2013/) under grant agreement No. 229517. This work was also supported by contributions of the European Union, Valle D'Aosta Region, and the Italian Minister for Work and Welfare. The National Radio Astronomy Observatory is operated by Associated Universities, Inc., under contract with the National Science Foundation. This research has made use of data obtained from the High-Energy Astrophysics Science Archive Research Center (HEASARC) provided by NASA's Goddard Space Flight Center; the SIMBAD database operated at CDS, Strasbourg, France; and the NASA/IPAC Extragalactic Database (NED) operated by the Jet Propulsion Laboratory, California Institute of Technology, under contract with the National Aeronautics and Space Administration. TOPCAT[17] (Taylor 2005) was used for the preparation and manipulation of the tabular data and the images. SAOImage DS9 was used extensively in this work for the preparation and manipulation of the images. SAOImage DS9 was developed by the Smithsonian Astrophysical Observatory.

Facilities: VLA, MERLIN, CXO (ACIS).

[17] http://www.star.bris.ac.uk/m̃bt/topcat/

APPENDIX A
IMAGES OF THE SOURCES

For all 93 3CR sources in our selected sample, radio morphologies are shown here as contours superposed on the re-gridded/smoothed X-ray events files. The FWHM of the Gaussian smoothing function and the binning factor are given in Table 7. X-ray event files were limited to the 0.5–7 keV band and re-binned to change the pixel size with a binning factor "f" (e.g., $f = 1/4$ produces pixels four times smaller than the native ACIS pixel of 0.″492). The labels on the color bar for each X-ray map are in units of counts/pixel. Also included in this table are the radio brightness of the lowest contour, the factor (usually 2 or 4) by which each subsequent contour exceeds the previous one, the frequency of the radio map, and the FWHM of the clean beam. The primary reason figures appear so different from each other is the wide range in angular size of the radio sources.

APPENDIX B
THE STATUS OF THE *CHANDRA* X-RAY 3CR OBSERVATIONS

Here we present the current status of the *Chandra* X-ray observations for the entire 3CR catalog, summarized in Table 8. For each 3CR source, we indicate the radio-to-optical classification indicating FRI and FRII radio galaxies, according to the Fanaroff & Riley criterion (Fanaroff & Riley 1974); quasars (i.e., QSRs); Seyfert galaxies (Sy); and BL Lac objects (BL). We indicate as "UND" those sources that, lacking optical spectroscopy, remain unidentified. Then, the most updated value of the redshift z is reported, together with the luminosity distance D_L and we also used a "cluster flag" to label sources that belong to a known galaxy cluster. Regarding the X-ray analysis, we report X-ray detections of radio components adopting the following symbols: k = jet knot; h = hotspot; l = lobe; and xcl for sources that belong to a galaxy cluster detected in the X-rays. Finally, the "*Chandra* flag" indicates if the source was already observed by *Chandra*.

REFERENCES

Abdo, A. A., Ackermann, M., Ajello, M., et al. 2011, ApJ, 726, 43
Balmaverde, B., Capetti, A., & Grandi, P. 2006, A&A, 451, 35
Balmaverde, B., Capetti, A., Grandi, P., et al. 2012, A&A, 545A, 143
Belsole, E., Worrall, D. M., Hardcastle, M. J., Birkinshaw, M., & Lawrence, C. R. 2004, MNRAS, 352, 924
Belsole, E., Worrall, D. M., Hardcastle, M. J., & Croston, J. H. 2007, MNRAS, 381, 1109
Bennett, A. S. 1962, MmRAS, 68, 163
Blanton, E. L., Randall, S. W., Douglass, E. M., et al. 2009, ApJL, 697, L95
Boschin, W. 2002, A&A, 396, 397
Brinkman, A. C., Kaastra, J. S., van der Meer, et al. 2002, A&A, 396, 761
Buttiglione, S., Capetti, A., Celotti, A., et al. 2009, A&A, 495, 1033
Chiaberge, M., Capetti, A., & Celotti, A. 2000, A&A, 355, 873
D'Abrusco, R., Massaro, F., Paggi, A., et al. 2013, ApJS, 206, 12
Donato, D., Sambruna, R. M., & Gliozzi, M. 2004, ApJ, 617, 915
Dunkley, J., Komatsu, E., Nolta, M. R., et al. 2009, ApJS, 180, 306
Edge, D. O., Shakeshaft, J. R., McAdam, W. B., Baldwin, J. E., & Archer, S. 1959, MmRAS, 68, 37
Erlund, M. C., Fabian, A. C., Blundell, Katherine, M., Celotti, A., Crawford, C. S., et al. 2006, MNRAS, 371, 29
Fabian, A. C., Sanders, J. S., Allen, S. W., et al. 2003, MNRAS, 344, L43
Fanaroff, B. L., & Riley, J. M. 1974, MNRAS, 167, P31
Gambill, J. K., Sambruna, R. M., Chartas, G., et al. 2003, A&A, 401, 505
Gilmour, R., Best, P., & Almaini, O. 2009, MNRAS, 392, 1509
Gliozzi, M., Sambruna, R. M., Eracleous, M., & Yaqoob, T. 2007, ApJ, 664, 88
Griffiths, R. E., Ptak, A., Feigelson, E. D., et al. 2000, Sci, 290, 1325
Haas, M., Leipski, C., Barthel, P., et al. 2014, ApJ, 790, 46
Hardcastle, M. J., Evans, D. A., & Croston, J. H. 2006, MNRAS, 370, 1893
Hardcastle, M. J., Evans, D. A., & Croston, J. H. 2009, MNRAS, 396, 1929
Hardcastle, M. J., Harris, D. E., Worrall, D. M., & Birkinshaw, M. 2004, ApJ, 612, 729
Hardcastle, M. J., Kraft, R. P., Worrall, D. M., et al. 2007, ApJ, 662, 166
Harwood, J. J., & Hardcastle, M. J. 2012, MNRAS, 423, 1368
Hiltner, P. R., & Roeser, H.-J. 2009, ApJS, 184, 398
Ho, L. C., & Minjin, K. 2009, ApJS, 184, 398
Hodges-Kluck, E. J., Reynolds, C. S., Cheung, C. C., & Miller, M. C. 2010, ApJ, 710, 1205
Hudson, D. S., Reiprich, T. H., Clarke, T. E., & Sarazin, C. L. 2006, A&A, 453, 433
Isobe, N., Seta, H., Gandhi, P., & Tashiro, M. S. 2011, ApJ, 727, 82
Kirkpatrick, C. C., McNamara, B. R., & Cavagnolo, K. W. 2011, ApJL, 731, L23
Kraft, R. P., Azcona, J., Forman, W. R., et al. 2006, ApJ, 639, 753
Kraft, R. P., Birkinshaw, M., Nulsen, P. E. J., et al. 2012, ApJ, 749, 19
Krawczynski, H. 2002, ApJ, 569L, 27
Lal, D. V., Kraft, R. P., Forman, W. R., et al. 2010, ApJ, 722, 1735
Lal, D. V., Kraft, R. P., Randall, S. W., et al. 2013, ApJ, 764, 83
Leahy, J. P., Black, A. R. S., Dennett-Thorpe, J., et al. 1997, MNRAS, 291, 20
Mackay, C. D. 1971, MNRAS, 154, 209
Massaro, F., Harris, D. E., & Cheung, C. C. 2011, ApJS, 197, 24
Massaro, F., Harris, D. E., Chiaberge, M., et al. 2009, ApJ, 696, 980
Massaro, F., Harris, D. E., Tremblay, G. R., et al. 2010, ApJ, 714, 589
Massaro, F., Harris, D. E., Tremblay, G. R., et al. 2013, ApJS, 203, 31
Massaro, F., Tremblay, G. R., Harris, D. E., et al. 2012, ApJS, 206, 7
Mazzotta, P., Kaastra, J. S., Paerels, F. B., et al. 2002, ApJL, 567, L37
McCarthy, I. G., Balogh, M. L., Babul, A., Poole, G. B., & Horner, D. J. 2004, ApJ, 613, 811
Miller, B. P., & Brandt, W. N. 2009, ApJ, 695, 755
Miller, B. P., Brandt, W. N., Schneider, D. P., et al. 2011, ApJ, 726, 20
Nulsen, P. E. J., Hambrick, D. C., & McNamara, B. R. 2005, ApJL, 625, L9
Nulsen, P. E. J., Li, Z., Forman, W. R., et al. 2013, ApJ, 775, 117
Reynolds, C. S., Brenneman, L. W., & Stocke, J. T. 2005, MNRAS, 357, 381
Salvati, M., Risaliti, G., Vron, P., & Woltjer, L. 2008, A&A, 478, 121
Siemiginowska, A., Burke, D. J., Aldcroft, et al. 2010, ApJ, 722, 102
Siemiginowska, A., LaMassa, S., Aldcroft, T. L., Bechtold, J., & Elvis, M. 2008, ApJ, 684, 811
Smith, H. E., Smith, E. O., & Spinrad, H. 1976, PASP, 88, 621
Smith, H. E., & Spinrad, H. 1980, PASP, 92, 553
Spinrad, H., Marr, J., Aguilar, L., & Djorgovski, S. 1985, PASP, 97, 932
Stockton, A., Fu, H., Henry, J. P., & Canalizo, G. 2006, ApJ, 638, 635
Sun, M. 2009, ApJ, 704, 1586
Taylor, M. B. 2005, in ASP Conf. Ser. 347, Astronomical Data Analysis Software and Systems XIV, ed. P. Shopbell, M. Britton, & R. Ebert (San Francisco, CA: ASP), 29
Tremblay, G. R., Chiaberge, M., Sparks, W. B., et al. 2009, ApJS, 183, 278
Vikhlinin, A., van Speybroeck, L., Markevitch, M., Forman, W. R., & Grego, L. 2002, ApJL, 578, L107
Wilkes, B. J., Kuraszkiewicz, J., Haas, M., et al. 2013, ApJ, 773, 15
Wilkes, B. J., Lal, D. V., Worrall, D. M., et al. 2012, ApJ, 745, 84
Worrall, D. M., Birkinshaw, M., Kraft, R. P., & Hardcastle, M. J. 2007, ApJL, 658, L79
Worrall, D. M., Hardcastle, M. J., Pearson, T. J., & Readhead, A. C. S. 2004, MNRAS, 347, 632